5-2008

Synthesis and Characterization of Copper(I) Halide and Nitrate Complexes of Heterocyclic Thioureas

Aakarsh Saxena
College of William and Mary

Synthesis and Characterization of Copper(I) Halide and Nitrate Complexes of Heterocyclic Thioureas

Table of Contents

Acknowledgements

I would like to thank Dr. Robert D. Pike for his time, commitment, and patience in writing this thesis and his constant explanations of chemistry. I also would like to thank the other members of my committee, Dr. Christopher J. Abelt, Dr. Randolph A. Coleman, and Prof. Jack Martin for giving their time and energy to consider this thesis. I am also grateful to The College of William and Mary Chemistry Department. I have learned so much in only a few short years, and that is entirely due to the dedication and encouragement each member of the department consistently shows. I am thankful for my family and friends, without whom I would not have completed this thesis. I finally thank the ACS Petroleum Research Fund for its financial support.

List of Figures

Figure *Page*

List of Tables

List of Reactions

Abstract

This thesis aims to characterize several novel copper(I) thiourea complexes of the form $(Cu^{I}X)_x(RNHCSNHR')_y$ (X = Cl, Br, I, or NO_3; R = 2-pyridyl, 3-pyridyl, 4-pyridyl, pyrimidyl, thiazole or benzothiazole; and R′ = phenyl or methyl; R = R′ = 2-pyridyl or 3-pyridyl). The synthesis and characterization of the novel heterocyclic thioureas from heterocyclic amines with phenyl- or methylisothiocyanate or CS_2 used in the copper(I) thiourea complexes mentioned above are also described. The chemical identity of each copper thiourea complex is verified by elemental analysis and/or X-ray crystallography. All complexes are analyzed for elemental analysis of copper, and several are also analyzed for carbon, hydrogen and nitrogen content. Additionally, many crystal structures are discussed, but due to difficulty in consistently obtaining X-ray quality crystals, not all complexes discussed have a known structure. X-ray crystal structures of seven new heterocyclic thioureas and nine new copper(I) thiourea complexes are reported.

1. Introduction

This research involves novel copper(I) thiourea complexes. Primarily, this thesis focuses on the synthesis and characterization of copper(I) salt complexes with heterocyclic thioureas. Additionally, the synthesis and characterization of the heterocyclic thioureas used in these copper(I) thiourea complexes are also described. The structural properties of the various compounds, which in many cases form long-range networks, are discussed. Potential applications of this research can be found in industrial catalysis (the development of heterogeneous carbonylation catalysts), in medicinal chemistry (carriers of small molecules such as nitric oxide to tumor cells), in storage and delivery (hemocyanin), and as luminescent material (due to $d^{10} \rightarrow d^9p^1$ -orbital interaction).

1.1 Thioureas

Ureas and thioureas are widely recognized for their ability to hydrogen-bond. In addition, they can act as ligands in coordination complexes. This combination has led to their increasing use in an array of self-assembled network materials [1, 2]. It is to be expected that incorporation of heterocyclic rings into thiourea molecules will produce an extended range of possible H-bonding interactions. A number of heterocyclic thiourea crystal structures have been determined [3-9]. However, virtually all of these structures feature a 2-pyridyl or related *ortho*-substituted nitrogen heterocycle. This heteroatom arrangement results in a highly favorable intramolecular H-bond, as illustrated in **I**. A few of the known structures show additional H-bonding, as represented in **II**–**V**. The six known compounds illustrated by **II** and **III** add to the ubiquitous internal H-bond an N–

H···S interaction, resulting in dimer formation [3, 5-8]. The "hydrogen-bonded" N···S distances in these species range from 3.256 to 3.379 Å. Although relatively weak, these thiocarbonyl H-bonding interactions are fairly common when the C=S is part of a resonance delocalized system and therefore is relatively long (>*ca.* 1.65 Å) [10]. Compounds **VI** and **V** make use of pendant heteroatom groups to form H-bonded chains, with the latter incorporating an H-bonded water molecule into the chain [6, 9]. Nevertheless, seven compounds that are closely related to **IV**, having pendant furan, thiophene, 2-methylpiperidine, and pyrrolidinone groups, adopt an internal H-bonding only structure, as illustrated by **I** [6].

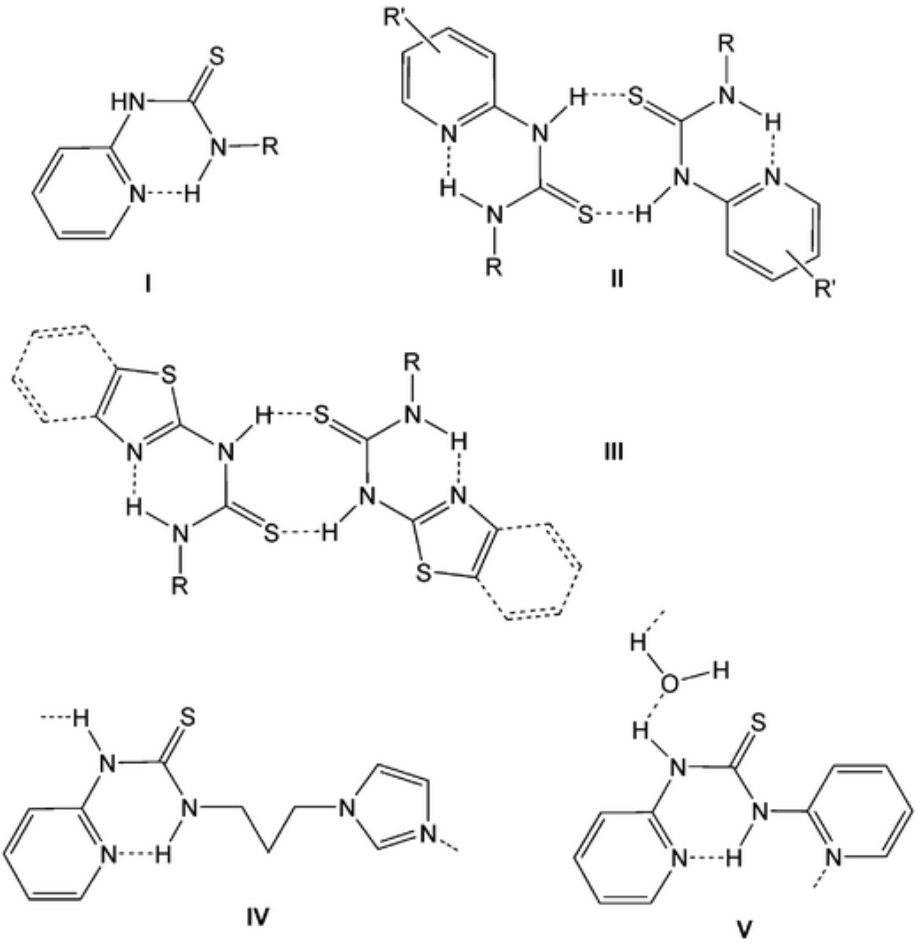

1.2 Copper(I) Network Formation

Copper has two common oxidation states; +1 and +2 [11]. These are both relatively stable. In addition to stability considerations, the physical and chemical properties vary considerably between the two oxidation states. Copper(II) has an electron configuration of $[Ar]3d^9$ [11], meaning it has a vacancy in its d-subshell. Because of ligand field splitting, the d orbitals in copper complexes are nondegenerate. The energy required to promote an electron into the higher energy orbital manifold corresponds to a wavelength in the visible light region. As a result, copper(II) compounds tend to be highly colored, generally blue or green. Copper(I) has the electron configuration $[Ar]3d^{10}$ [11], meaning it has no vacancies in its d orbitals. Electronic promotion cannot occur within the d subshell, so the energy required for excitation is greater than that of visible light. This results in copper(I) compounds typically being white.

The coordination chemistry of copper(II) has been well documented, but studies focusing primarily on copper(I) are less common. By expanding the knowledge base of the range of copper(I) compounds that form, one can more accurately predict and pursue potential applications of such molecules. The results discussed herein rest largely upon new crystal structure determinations. Although the prevailing coordination environment of copper(I) is 4-coordinate, cases of both 2- and 3-coordination have been reported. This flexible coordination ability is derived at least partially from the lack of crystal field-based d orbital splitting for copper(I) and is often sterically controlled. The most common geometry for a 4-coordinate copper(I) is tetrahedral, illustrated in Figure 1.

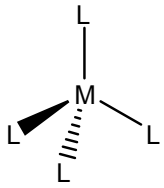

Figure 1: A tetrahedral coordination environment

In recent years large numbers of framework solids have been structurally characterized; the vast majority makes use of hydrogen bonding or ligand-to-metal coordinative bonding to link the individual components [12]. Coordination compounds with peripheral hydrogen bonding substituents have been used to assemble infinite frameworks of one, two, and three dimensions, The propagation of 1D, 2D and 3D network depends on the nature of the metal ion, the number of hydrogen bonding substituents used, and the nature and placement of the hydrogen bonding substituents [13]. Examples of 1D, 2D, and 3D structures are shown in Figure 2, 3, and 4:

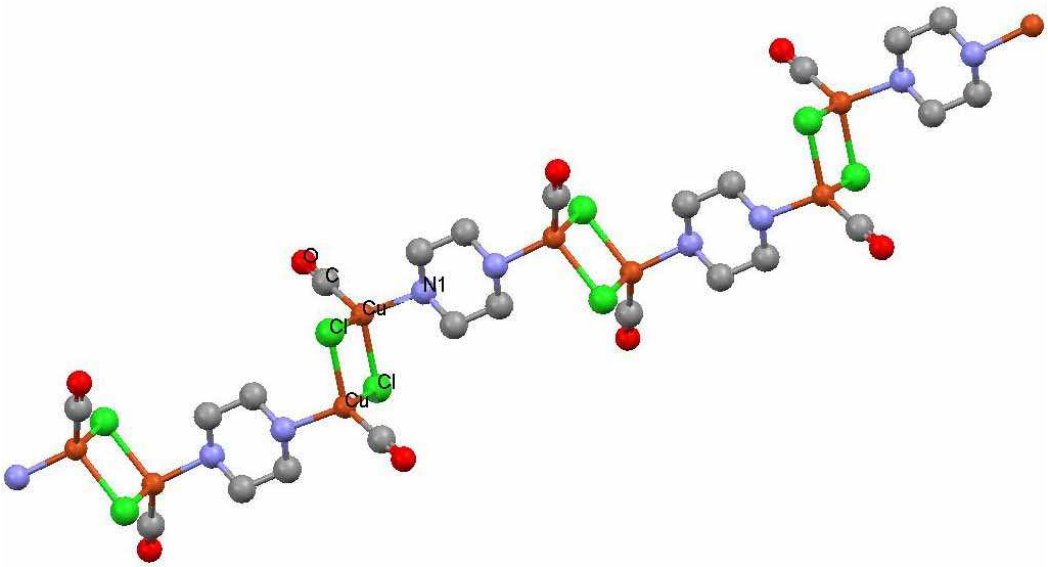

Figure 2: X-ray structure of 1D, $(CuCl)_2(Piperazine)(CO)_2$ [14]. Hydrogen atoms omitted for clarity. Atom color scheme for all X-ray structures:- Cu: Orange. Cl: Green. Br: Brown. N: Blue. O: Red. C: Grey. H: White.

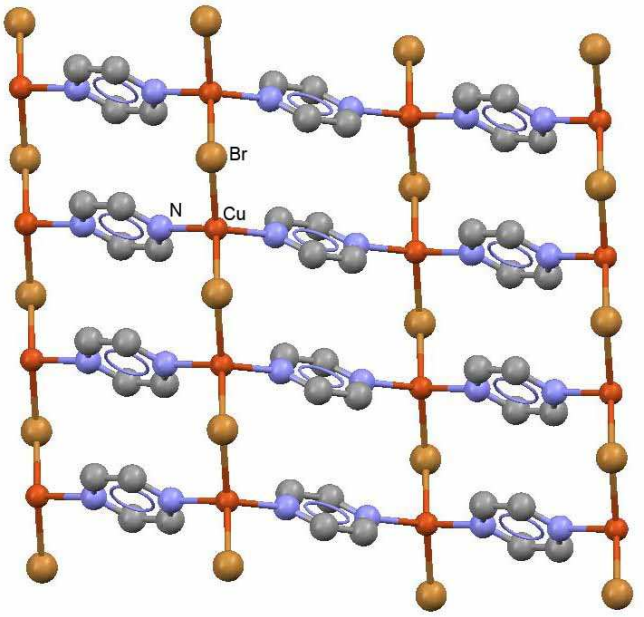

Figure 3: X-ray structure of 2D, CuBr(Pyrazine) [15]. Hydrogen atoms omitted for clarity.

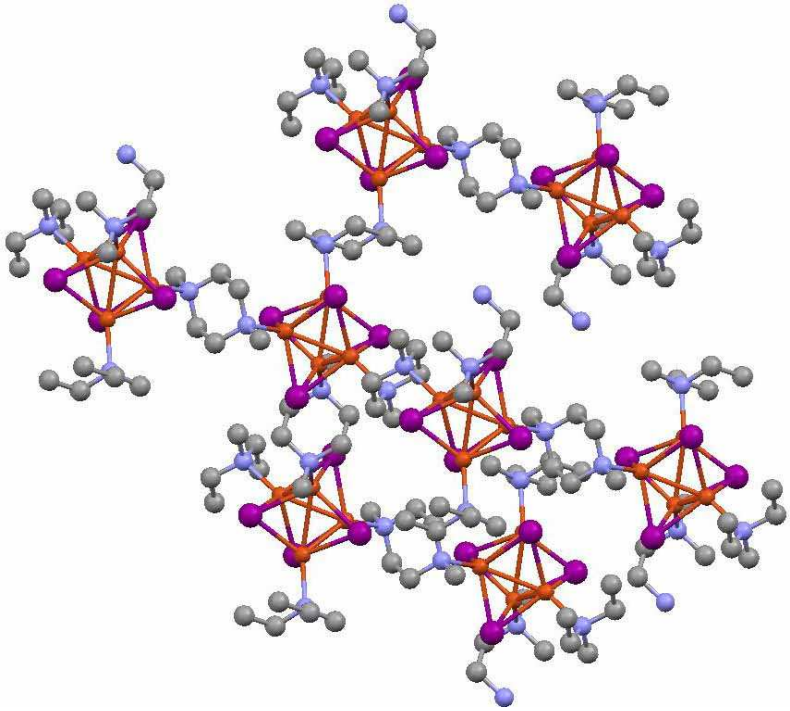

Figure 4: $(CuI)_2$(N,N'-dimethylpiperazine) [16]

One would expect 2-coordinate copper(I) complexes to form 1D linear chains, 3-coordinate copper(I) complexes to form 2D sheets, and 4-coordinate copper(I) complexes to form 3D structures owing to their geometry. Yet, many exceptions to this statement have been found and are also reported in this paper.

In some cases the frameworks do generate spacious voids, cavities, and channels which may account for more than half the volume of the crystal. These large spaces are usually occupied by highly disordered, essentially liquid solvent [12]. Many supramolecular chemists and crystal engineers are preoccupied by a quest for space, the goal being to create materials to store molecules or ions, to develop chemical sensors, or to use the channels or cavities as templates for catalysis. In order to create space, one must have a strategy for assembly, a basis for generating a host network. One danger is that even if one is successful in creating the desired framework, the networks may themselves occupy intra-net space through interpenetration [13]. An example to illustrate the formation of cavities is shown in Figure 5 with zinc metal. The large circular voids seen in Figure 5 are ideal for the purposes discussed previously.

Another important aspect for consideration is π-stacking interaction, which refers to a stacked arrangement of aromatic molecules interacting through aromatic interactions, as shown in Figure 6.

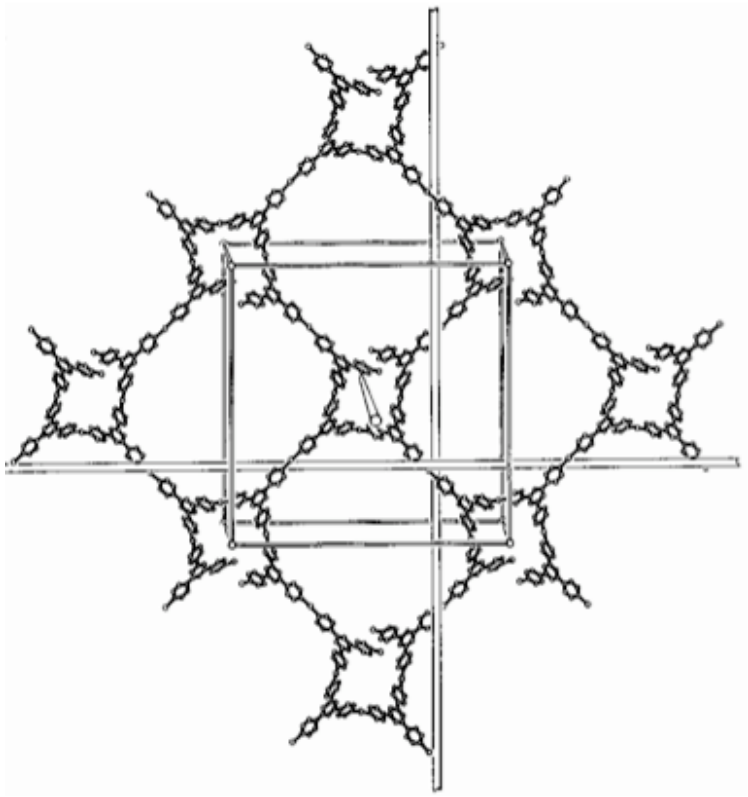

Figure 5: One of the eight (10, 3)-a nets present in $[Zn(tpt)_{2/3}](SiF_6)\bullet 2H_2O\bullet CH_3OH$ (tpt = 2,4,6-tris(4-pyridyl)-1,3,5-triazine) [13].

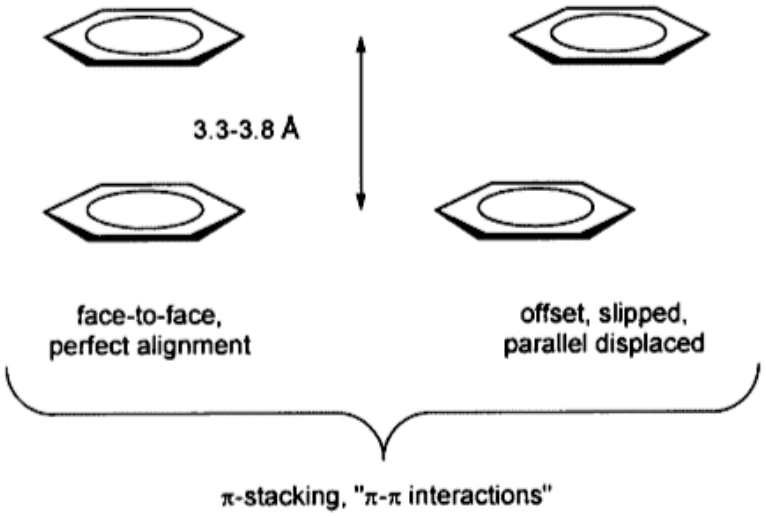

Figure 6: Orientation of π- π interactions [17].

A $\pi - \pi$ interaction is a non-covalent interaction between organic compounds containing aromatic moieties. Such interactions are caused by intermolecular overlapping of p-orbitals in π-conjugated systems, so they become stronger as the number of π-electrons increase. In an article by Janiak [17] it was shown that perfect face-to-face alignment is seldom seen and a more commonly encountered phenomenon is that of an offset, slipped, parallel-displaced setting. Also in the article it was shown that for any significant $\pi - \pi$ interaction to occur, the aromatic rings were required to be at a distance of 3.3-3.8 Å from each other. π-Stacking plays an important role in determining the structure and geometry of metal-ligand complexes and thus must be considered. X-ray diffraction studies can provide us with clear indications of such interactions.

1.3 Copper(I) Halide and Nitrate Thiourea Complexes

There has been considerable research into copper salt thiourea complexes, but work using heterocyclic thiourea is almost unknown. The thiourea ligands used in this research are in Figure 7. Thioureas are potentially interesting ligands because of the accessibility of several heteroatoms. Each of these areas of electron density represents a possible binding site for metal(s). Specifically, there are two lone pairs on each sulfur, allowing possible bridging μ_2-S, an arrangement which facilitates polymer construction. The two nitrogen atoms on either side of the thiocarbonyl can also potentially bind metal centers. However, the thioureas shown in Figure 7 have additional nitrogen atom(s) introduced.

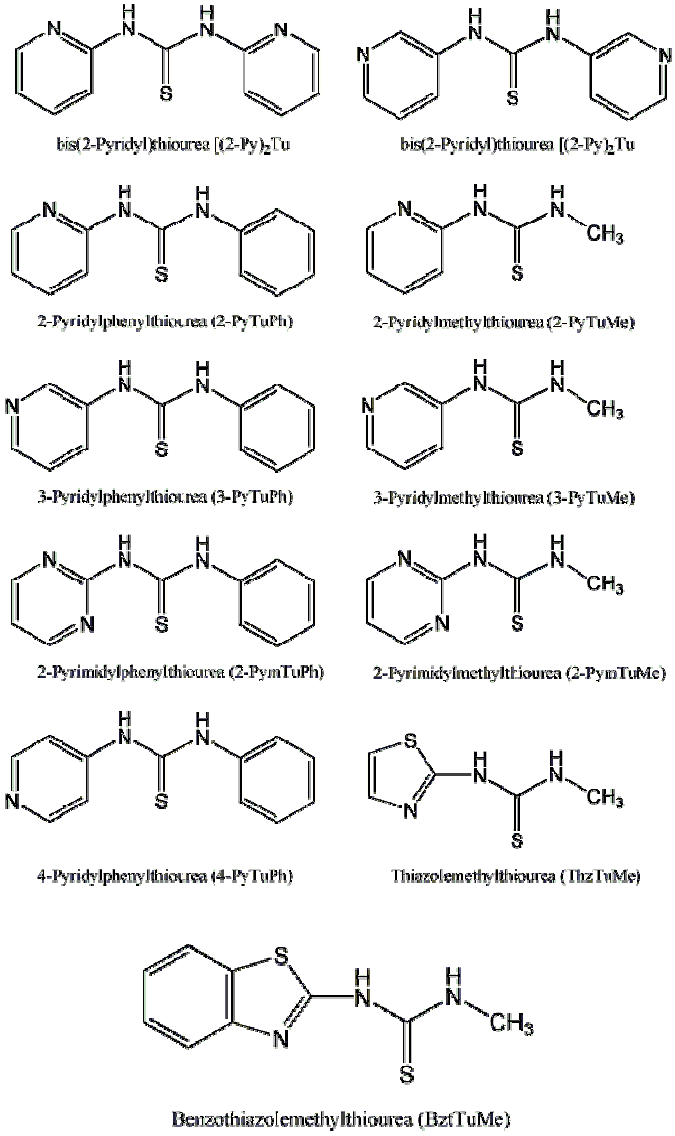

Figure 7: Thiourea Structures

The pyridyl or pyrimidyl nitrogen atoms allow not only for an additional binding site, but also for the possibility of chelation. Moreover, the crystals of heterocyclic thioureas show a significant amount of structure from both inter- and intramolecular hydrogen bonding which is discussed in section 3.1.

In the following project we set out to produce copper(I) halide and nitrate complexes of heterocyclic thioureas. These complexes were characterized in terms of both stoichiometry and structure, and general trends were drawn from these results.

2. Experimental

2.1 General

All reagents were purchased from Aldrich or Acros and used without purification, except for CuCl and CuBr, which were recrystallized to remove Cu(II) impurities. Melting point data for the thioureas were recorded on a MelTemp apparatus and are reported uncorrected. NMR data were recorded on a Varian Mercury 400 instrument (s = singlet, d = doublet, t = triplet, br = broad, v br = very broad, J = coupling constant; Py = pyridyl, Pym = 2-pyrimidyl, Thz = 2-thiazolyl, Bzt = 2-benzothiazolyl; for numbering of heterocycles see **1**–**10**). IR spectra were recorded using a Digilab FTS-7000 series FTIR as KBr pellets (s = strong intensity, m = medium, w = weak, br = broad). Analyses for C, H, and N were carried out by Atlantic Microlabs, Norcross, GA. Analyses for Cu were carried out using a Perkin-Elmer AAnalyst 700 atomic absorption instrument. The compounds were prepared by measuring roughly 10-12 mg of the complex in about 1 mL of HNO_3, at room temperature, followed by heating the mixture at about 50 ^{o}C degrees Celsius for roughly 10 minutes. Using ultra-filtered deionized quality water (UFDI), the mixture was transferred to a 100 mL volumetric flask, then diluted a second time to achieve a concentration acceptable to the instrument. Standards were prepared by diluting a 1000 ppm stock solution of $Cu(NO_3)_2$ to 500, 1000, 1500, 2000, and 2500 ppb in UFDI. Absorption measurements were made at 324 nm.

2.2 Heterocyclic Thioureas

2.2.1 Synthesis

2.2.1.1 Synthesis of N-(2-Pyridyl)-N′-methylthiourea

2-Aminopyridine (0.94 g, 10.0 mmol) was dissolved in 15 mL pyridine. Methyl isothiocyanate (1.10 g, 15.0 mmol) was added, forming a clear, yellow solution. The mixture was stirred overnight under N_2. The red-brown solution was concentrated and cooled, producing a precipitate. The off-white product was isolated by vacuum filtration, stirred in water overnight to remove residual 2-aminopyridine, and was dried *in vacuo* (0.84 g, 50.23%). m.p.: 144–146 °C. ^{1}H NMR (400 MHz, $CDCl_3$) δ 11.69 (s, 1H, NH), 9.30 (s, 1H, NH), 8.17, (d, J = 3.5, 1H, H_{Py-6}), 7.64 (dd, J = 8.2 Hz, 1H, H_{Py-5}), 6.95 (dd, J = 6.3 Hz, 1H, H_{Py-4}), 6.90 (d, J = 8.6, 1H, H_{Py-3}), 3.29 (s, 3H, CH_3). $^{13}C\{^1H\}$ NMR (100 MHz, $CDCl_3$) δ 180.42, 153.35, 146.08, 138.95, 118.15, 112.04, 32.49. Anal. Calcd. for $C_7H_9N_3S$ C, 50.28; H, 5.42; N, 25.13. Found: C, 50.33; H, 5.48; N, 25.05. IR: 3203 (m, br), 3039 (m), 1599 (s), 1571 (w), 1545 (s), 1483 (s), 1449 (m, br), 1348 (w), 1318 (m), 1244 (m), 1219 (m), 1153 (m), 1057 (s), 769 (s), 704 (m, br), 628 (m).

2.2.1.2 Synthesis of N-(3-Pyridyl)-N′-phenylthiourea

3-Aminopyridine (4.71 g, 50.0 mmol) was dissolved in 60 mL EtOH. Phenyl isothiocyanate (6.76 g, 50.0 mmol) was added, forming a clear, colorless solution. The mixture was stirred overnight under N_2 leading to formation of a precipitate. The white product was isolated by vacuum filtration, was washed with pentane, and was dried *in vacuo* (9.62 g, 83.9%). m.p.: 156–158 °C. ^{1}H NMR (400 MHz, $CDCl_3$) δ 8.50 (d, J = 2.4 Hz, 1H, H_{Py-2}), 8.47 (d, J = 4.7 Hz, 1H, H_{Py-4}), 8.07 (d, J = 8.6 Hz, 1H, H_{Py-6}), 7.94 (s, 1H, NH) 7.62 (s, 1H, NH), 7.50 (7, J = 7.8 Hz, 2H, H_{Ph-m}), 7.36 (m, 4H, H_{Py-5}, $H_{Ph-o,p}$). $^{13}C\{^1H\}$ NMR (100 MHz, $CDCl_3$) δ 180.76, 146.19, 145.51, 138.29, 136.07, 132.05, 129.28, 126.23, 124.88, 123.25. Anal. Calcd. for $C_{12}H_{11}N_3S$ C, 62.86; H, 4.84; N, 18.33. Found: C, 62.97; H, 4.87; N, 18.39. IR: 3150 (s, br), 2977 (m, br), 2872 (m, br), 1535 (s),

1511 (s), 1489 (m), 1379 (m), 1231 (m), 1198 (m), 1099 (w), 1024 (m), 735 (m), 710 (m), 691 (m), 647 (m), 615 (m).

2.2.1.3 Synthesis of N-(3-Pyridyl)-N′-methylthiourea

3-Aminopyridine (0.94 g, 10.0 mmol) was dissolved in 15 mL pyridine. Methyl isothiocyanate (1.10 g, 15.0 mmol) was added, forming a clear, yellow solution. The mixture was stirred overnight under N_2. The red-brown solution was concentrated and cooled, producing a precipitate. The off-white product was isolated by vacuum filtration, and was dried *in vacuo* (1.37 g, 82.00%). m.p.: 137–139 °C. ^{1}H NMR (400 MHz, $CDCl_3$) δ 10.09 (s, 1H, NH), 9.67 (s, 1H, NH), 8.56, (br s, 1H, H_{Py-2}) 8.30 (d, J = 4.7 Hz, 1H, H_{Py-6}), 7.90 (d, J = 8.2 Hz, 1H, H_{Py-4}), 7.34 (dd, J = 8.2, 1H, H_{Py-5}), 2.95 (s, 3H, CH_3). $^{13}C\{^1H\}$ NMR (100 MHz, $CDCl_3$) δ 187.16, 149.91, 149.76, 141.55, 135.53, 128.23, 36.53. Anal. Calcd. for $C_7H_9N_3S$ C, 50.28; H, 5.42; N, 25.13. Found: C, 50.10; H, 5.46; N, 24.91. IR: 3336 (s), 3195 (m, br), 3011 (m, br), 1523 (s, br), 1478 (s), 1318 (m), 1285 (s), 1234 (w), 1052 (m), 1020 (m), 810 (w), 767 (w), 704 (w).

2.2.1.4 Synthesis of N-(4-Pyridyl)-N′-phenylthiourea

4-Aminopyridine (1.88 g, 20.0 mmol) was dissolved in 20 mL pyridine. Phenyl isothiocyanate (3.38 g, 25.0 mmol) was added, forming a clear, yellow solution. The mixture was stirred overnight under N_2 leading to formation of a precipitate. The white product was isolated by vacuum filtration, stirred in water overnight to remove residual 4-aminopyridine, and was dried *in vacuo* (3.54 g, 77.1%). m.p.: 139–141 °C. ^{1}H NMR (400 MHz, $CDCl_3$) δ 9.44 br (s, 1H, NH), 8.76 (br s, 1H, NH), 8.46 (d, J = 4.7 Hz, 2H, $H_{Py-3,5}$), 7.71 (d, J = 4.7 Hz, 2H, $H_{Py-2,6}$), 7.48, (d, J = 8.6 Hz, 2H, H_{Ph-o}), 7.38 (t, J = 7.4 Hz, 2H, H_{Ph-m}), 7.23 (t, J = 7.4 Hz, 1H, H_{Ph-p}). $^{13}C\{^1H\}$ NMR (100 MHz, $CDCl_3$)

δ 150.75, 130.61, 129.87, 128.35, 127.42, 125.63, 125.53, 116.49. Anal. Calcd. for $C_{12}H_{11}N_3S$ C, 62.86; H, 4.84; N, 18.33. Found: C, 63.05; H, 4.87; N, 18.05. IR: 3160 (s, br), 2992 (m, br), 2951 (m, br), 2926 (m, br), 1593 (s), 1533 (s), 1511 (s), 1485 (s), 1413 (s), 1364 (s), 1287 (m), 1226 (m), 1190 (s), 1004 (w), 777 (s), 692 (m), 642 (m), 628 (m).

2.2.1.5 Synthesis of N-(2-Pyrimidyl)-N′-phenylthiourea

2-Aminopyrimidine (4.76 g, 50.0 mmol) was dissolved in 20 mL pyridine. Phenyl isothiocyanate (8.12 g, 60.0 mmol) was added, forming a clear, yellow solution. The mixture was stirred overnight under N_2 leading to formation of a precipitate. The white product was isolated by vacuum filtration, washed with diethyl ether, and was dried *in vacuo* (4.82 g, 41.9%). m.p.: 188–191 °C. ^{1}H NMR (400 MHz, $CDCl_3$) δ 12.99 (s, 1H, NH), 9.95 (s, 1H, NH), 8.79 (s, 2H, $H_{Pym-3,5}$), 7.67 (d, J = 7.8 Hz, 2H, H_{Ph-o}), 7.43 (7, J = 7.4 Hz, 2H, H_{Ph-m}), 7.30 (t, J = 6.3 Hz, 1H, H_{Pym-4}), 7.05 (d, J = 4.7 Hz, 1H, H_{Ph-p}). ^{13}C{^{1}H} NMR (100 MHz, $CDCl_3$) δ 179.03, 157.64, 138.70, 129.02, 126.75, 125.15, 115.67. Anal. Calcd. for $C_{11}H_{10}N_4S$ C, 57.37; H, 4.38; N, 24.33. Found: C, 57.58; H, 4.33; N, 24.30. IR: 3209 (m, br), 3173 (m, br), 3028 (m, br), 1593 (m), 1546 (s), 1518 (s), 1443 (m), 1416 (s), 1350 (w), 1195 (m), 1559 (m), 800 (m), 692 (m).

2.2.1.6 Synthesis of N-(2-Pyrimidyl)-N′-methylthiourea

2-Aminopyrimidine (2.38 g, 25.0 mmol) was dissolved in 25 mL pyridine. Methyl isothiocyanate (2.56 g, 35.0 mmol) was added, forming a clear, yellow solution. The mixture was stirred overnight under N_2. The red-brown solution was concentrated and cooled, producing a precipitate. The off-white product was isolated by vacuum filtration, was washed with diethyl ether, and was dried *in vacuo* (3.24 g, 76.9%). m.p.: 212–214 °C. ^{1}H NMR (400 MHz, $CDCl_3$) δ 11.12 (s, 1H, NH), 9.99 (s, 1H, NH), 8.77, (br s,

2H, $H_{Pym-3,5}$) 7.00 (t, J = 4.7 Hz, 1H, H_{Pym-4}), 3.29 (t, J = 4.7 Hz, 3H, CH_3). $^{13}C\{^1H\}$ NMR (100 MHz, $CDCl_3$) δ 180.78, 157.88, 115.37, 32.66. Anal. Calcd. for $C_6H_8N_4S$ C, 42.84; H, 4.79; N, 33.31. Found: C, 42.94; H, 4.83; N, 33.15. IR: 3230 (m, br), 3165 (w, br), 3071 (m, br), 1578 (s), 1529 (m), 1426 (m), 1359 (w), 1333 (w), 1213 (m), 1143 (w), 1051 (m), 818 (m), 792 (m), 644 (m).

2.2.1.7 Synthesis of N-(2-Thiazolyl)-N′-methylthiourea

2-Aminothiazole (2.50 g, 25.0 mmol) was dissolved in 25 mL pyridine. Methyl isothiocyanate (2.19 g, 30.0 mmol) was added, forming a clear, brown solution. The mixture was stirred overnight under N_2. The brown solution was evaporated, leaving a viscous brown oil which solidified under vacuum. The light brown product was washed with diethyl ether, and was dried in vacuo (3.24 g, 76.9%). m.p.: 164–166 °C. ^1H NMR (400 MHz, $CDCl_3$) δ 11.00 (br s, 1H, NH), 10.81 (br s, 1H, NH), 7.32 (d, J = 3.5 Hz, 1H, H_{Thz-5}), 6.85 (d, J = 3.5 Hz, 1H, H_{Thz-4}), 3.26 (d, J = 4.7 Hz, 3H, CH_3). $^{13}C\{^1H\}$ NMR (100 MHz, $CDCl_3$) δ 178.61, 162.11, 137.80, 111.52, 32.27. Anal. Calcd. for $C_5H_7N_3S_2$ C, 34.66; H, 4.07; N, 24.25. Found: C, 34.95; H, 4.11; N, 24.06. IR: 3157 (m, br), 3103 (m), 3061 (m, br), 2968 (m, br), 1594 (s), 1561 (s), 1517 (s), 1459 (m), 1359 (w), 1242 (s), 1163 (m), 1112 (w), 1076 (w), 1053 (m), 691 (m), 607 (w).

2.2.1.8 Synthesis of N-(2-Benzothiazolyl)-N′-methylthiourea

2-Aminobenzothiazole (3.76 g, 25.0 mmol) was dissolved in 25 mL pyridine. Methyl isothiocyanate (2.56 g, 35.0 mmol) was added, forming a clear, yellow solution. The mixture was stirred overnight under N_2. The red-brown solution was evaporated to dryness, producing a reddish brown impure product. The yellow product was isolated by vacuum filtration, stirred in diethyl ether, and was dried *in vacuo* (3.43 g, 61.40%). m.p.:

185–188 °C. ^{1}H NMR (400 MHz, $CDCl_3$) δ 11.12 (s, 1H, NH), 10.95 (br s, 1H, NH), 7.71 (t, J = 8.2 Hz, 2H, $H_{Bzt-5,8}$), 7.41 (dd, J = 7.4 Hz, 1H, $H_{Bzt-6/7}$), 7.28 (dd, J = 7.4 Hz, 1H, $H_{Bzt-7/6}$), 3.34 (d, J = 4.7 Hz, 3H, CH_3). $^{13}C\{^{1}H\}$ NMR (100 MHz, $CDCl_3$) δ 178.99, 160.54, 149.61, 130.09, 126.71, 124.58, 121.49, 120.78, 31.34. Anal. Calcd. for $C_9H_9N_3S_2$ C, 48.41; H, 4.06; N, 18.82. Found: C, 48.19; H, 4.12; N, 18.96. IR: 3180 (m, br), 3049 (m, br), 1566 (s, br), 1520 (s), 1455 (m), 1439 (m), 1236 (m, br), 1077 (w), 912 (w), 750 (m), 687 (w).

2.2.1.9 Synthesis of N,N′-Bis(2-pyridyl)thiourea

2-Aminopyridine (4.71 g, 50.0 mmol) was dissolved in 20 mL pyridine. Carbon disulfide (7.71 g, 100 mmol) was added, forming a clear, yellow solution. The mixture was refluxed overnight under N_2. The solution was concentrated and cooled, producing a precipitate. The off-white product was isolated by vacuum filtration, stirred in water overnight to remove residual 2-aminopyridine, and was dried *in vacuo* (4.02 g, 69.8%). m.p.: 155–158 °C. ^{1}H NMR (400 MHz, $CDCl_3$) δ 9.4 (v br s, 2H, NH), 8.6 (v br s, 2H, H_{Py-3}), 8.40 (br s, 2H, H_{Py-4}), 7.72 (br s, 2H, H_{Py-6}), 7.07 (br s, 2H, H_{Py-5}). $^{13}C\{^{1}H\}$ NMR (100 MHz, $CDCl_3$) δ 176.28, 151.52, 146.96 & 145.37 (partially coalesced), 136.79 (coalesced, br), 119.24 & 117.86 (partially coalesced), 115.60 & 111.53 (partially coalesced). Anal. Calcd. for $C_{11}H_{10}N_4S_1$ C, 57.37; H, 4.38; N, 24.33. Found: C, 57.65; H, 4.29; N, 24.50. IR: 3462 (s, br), 3235 (m), 1601 (s), 1561 (s), 1524 (s), 1471 (s), 1421 (s), 1351 (s), 1182 (m), 1146 (m), 771 (m).

2.2.1.10 Synthesis of N,N′-Bis(3-pyridyl)thiourea

3-Aminopyridine (4.71 g, 50.0 mmol) was dissolved in 20 mL pyridine. Carbon disulfide (7.71 g, 100 mmol) was added, forming a clear, yellow-brown solution. The

mixture was stirred overnight under N_2 leading to formation of a precipitate. The white product was isolated by vacuum filtration, washed with diethyl ether, and was dried *in vacuo* (4.36 g, 75.7%). m.p.: 169–172 °C. ^{1}H NMR (400 MHz, $CDCl_3$) δ 10.10 (s, 2H, NH), 8.63 (d, J = 2.7 Hz, 2H, H_{Py-2}), 8.36 (d, J = 3.6 Hz, 2H, H_{Py-4}), 7.95 (d, J = 8.2 Hz, 2H, H_{Py-6}), 7.39 (dd, J = 8.2, 4.7 Hz, 2H, H_{Py-5}). $^{13}C\{^1H\}$ NMR (100 MHz, $CDCl_3$) δ 180.64, 145.32, 145.27, 135.82, 131.38, 123.07. Anal. Calcd. for $C_{11}H_{10}N_4S_1$ C, 57.37; H, 4.38; N, 24.33. Found: C, 57.61; H, 4.39; N, 24.29. IR: 3208 (w), 3166 (w), 3208 (w), 2978 (s, br), 2936 (m, br), 2787 (w, br), 1599 (m), 1582 (m), 1535 (m), 1473 (w), 1417 (s), 1314 (m), 1276 (s), 1254 (m), 1024 (w), 762 (w), 719 (s), 640 (w).

2.2.2 X-ray diffraction Studies

X-ray quality crystals were grown by slow evaporation or diethyl ether layering of acetone solutions. Crystals were mounted on glass fibers. All measurements were made using graphite-monochromated Cu Kα radiation on a Bruker-AXS three-circle diffractometer, equipped with a SMART APEX II CCD detector. Initial space group determination was based on a matrix consisting of 120 frames. The data were reduced using SAINT+ [18], and empirical absorption correction applied using SADABS [19].

Structures were solved using direct methods. Least-squares refinement for all structures was carried out on F^2. The non-hydrogen atoms were refined anisotropically. All hydrogen atoms in each structure were located by standard difference Fourier techniques and were refined with isotropic thermal parameters. Structure solution, refinement and the calculation of derived results were performed using the SHELXTL package of computer programs [20]. Packing diagrams were produced using Mercury

[21]. Details of the X-ray experiments and crystal data are summarized in Table 1. Selected bond lengths and bond angles are given in Table 2, a summary of hydrogen-bonds is provided in Table 3, and a summary of interplanar angles is found in Table 4.

2.3 Copper(I) Thiourea Complexes

2.3.1 Synthesis

2.3.1.1 Preparation of CuCl Complexes

2.3.1.1.1 Synthesis of (CuCl)(2-PyTuPh)$_2$

Copper(I) chloride (99 mg, 1.00 mmol) was dissolved in 25 mL MeCN under nitrogen. 2-PyTuPh (229 mg, 1.00 mmol) was added as a solid. The resulting suspension was stirred under nitrogen for roughly an hour at room temperature. This resulted in a white precipitate. The solvent was removed via filtration, and the solid was washed with diethyl ether. The white solid was dried under a vacuum overnight (184 mg, 68.5% yield).

2.3.1.1.2 Synthesis of (CuCl)$_2$(2-PyTuMe)$_3$

Copper(I) chloride (99 mg, 1.00 mmol) was dissolved in 25 mL MeCN under nitrogen. 2-PyTuMe (167 mg, 1.00 mmol) was added as a solid. The resulting suspension was stirred under nitrogen for roughly an hour at room temperature. This resulted in a white precipitate. The solvent was removed via filtration, and the solid was washed with diethyl ether. The white solid was dried under a vacuum overnight (175 mg, 75.1% yield).

2.3.1.1.3 Synthesis of CuCl(3-PyTuPh)$_3$

Copper(I) chloride (99 mg, 1.00 mmol) was dissolved in 25 mL MeCN under nitrogen. 3-PyTuPh (229 mg, 1.00 mmol) was added as a solid. The resulting suspension was stirred under nitrogen for roughly an hour at room temperature. This resulted in a yellow precipitate. The solvent was removed via filtration, and the solid was washed with diethyl ether. The yellow solid was dried under a vacuum overnight (213 mg, 81.3% yield).

2.3.1.1.4 Synthesis of CuCl(3-PyTuMe)

Copper(I) chloride (99 mg, 1.00 mmol) was dissolved in 25 mL MeCN under nitrogen. 3-PyTuMe (167 mg, 1.00 mmol) was added as a solid. The resulting suspension was stirred under nitrogen for roughly an hour at room temperature. This resulted in a white precipitate. The solvent was removed via filtration, and the solid was washed with diethyl ether. The white solid was dried under a vacuum overnight (194 mg, 72.9% yield).

2.3.1.1.5 Synthesis of CuCl(4-PyTuPh)

Copper(I) chloride (198 mg, 2.00 mmol) was dissolved in 20 mL MeCN under nitrogen. 4-PyTuPh (459 mg, 2.00 mmol) was suspended in 15 mL MeCN and injected into the CuCl solution. The resulting suspension was stirred under nitrogen for roughly an hour at room temperature. This resulted in a yellow precipitate. The solvent was removed via filtration, and the solid was washed with diethyl ether. The yellow solid was dried under a vacuum overnight (486 mg, 74.0% yield).

2.3.1.1.6 Synthesis of $CuCl(PymTuPh)_2$

Copper(I) chloride (99 mg, 1.00 mmol) was dissolved in 25 mL MeCN under nitrogen. PymTuPh (229 mg, 1.00 mmol) was added as a solid. The resulting suspension

was stirred under nitrogen for roughly an hour at room temperature. This resulted in a white precipitate. The solvent was removed via filtration, and the solid was washed with diethyl ether. The white solid was dried under a vacuum overnight (237 mg, 85.1% yield).

2.3.1.1.7 Synthesis of $CuCl(PymTuMe)_4$

Copper(I) chloride (99 mg, 1.00 mmol) was dissolved in 25 mL MeCN under nitrogen. PymTuMe (167 mg, 1.00 mmol) was added as a solid. The resulting suspension was stirred under nitrogen for roughly an hour at room temperature. This resulted in a brown precipitate. The solvent was removed via filtration, and the solid was washed with diethyl ether. The brown solid was dried under a vacuum overnight (164 mg, 85.0% yield).

2.3.1.1.8 Synthesis of CuCl(BztTuMe)•0.5MeCN

Copper(I) chloride (198 mg, 2.00 mmol) was dissolved in 15 mL MeCN under nitrogen. BztTuMe (447 mg, 2.00 mmol) was added as a solid. The resulting suspension was stirred under nitrogen for roughly an hour at room temperature. This resulted in a yellow-white precipitate. The solvent was removed via filtration, and the solid was washed with diethyl ether. The yellow-white solid was dried under a vacuum overnight (548 mg, 87.6% yield).

2.3.1.1.9 Synthesis of $(CuCl)_2(ThzTuMe)_3$

Copper(I) chloride (198 mg, 2.00 mmol) was dissolved in 20 mL MeCN under nitrogen. ThzTuPh (347 mg, 2.00 mmol) was suspended in 15 mL MeCN and injected into the CuCl solution. The resulting suspension was stirred under nitrogen for roughly an hour at room temperature. This resulted in a white precipitate. The solvent was removed

via filtration, and the solid was washed with diethyl ether. The white solid was dried under a vacuum overnight (274 mg, 19.4% yield).

2.3.1.1.10 Synthesis of $(CuCl)_2[(2\text{-}Py)_2Tu]_3$

Copper(I) chloride (198 mg, 2.00 mmol) was dissolved in 20 mL MeCN under nitrogen. $(2\text{-}Py)_2Tu$ (461 mg, 2.00 mmol) was suspended in 15 mL MeCN and injected into the CuCl solution. The resulting suspension was stirred under nitrogen for roughly an hour at room temperature. This resulted in a yellow precipitate. The solvent was removed via filtration, and the solid was washed with diethyl ether. The yellow solid was dried under a vacuum overnight (407 mg, 68.7% yield).

2.3.1.1.11 Synthesis of $(CuCl)[(3\text{-}Py)_2Tu]_4$

Copper(I) chloride (198 mg, 2.00 mmol) was dissolved in 20 mL MeCN under nitrogen. $(2\text{-}Py)_2Tu$ (461 mg, 2.00 mmol) was suspended in 15 mL MeCN and injected into the CuCl solution. The resulting suspension was stirred under nitrogen for roughly an hour at room temperature. This resulted in a green precipitate. The solvent was removed via filtration, and the solid was washed with diethyl ether. The pale green solid was dried under a vacuum overnight (418 mg, 81.9% yield).

2.3.1.2 Preparation of CuBr Complexes

2.3.1.2.1 Synthesis of CuBr(2-PyTuPh)•MeCN

Copper(I) bromide (143 mg, 1.00 mmol) was dissolved in 25 mL MeCN under nitrogen. 2-PyTuPh (229 mg, 1.00 mmol) was added as a solid. The resulting suspension was stirred under nitrogen for roughly an hour at room temperature. This resulted in a white precipitate. The solvent was removed via filtration, and the solid was washed with

diethyl ether. The white solid was dried under a vacuum overnight (321 mg, 77.6% yield).

2.3.1.2.2 Synthesis of CuBr(2-PyTuMe)•0.5 MeCN

Copper(I) bromide (143 mg, 1.00 mmol) was dissolved in 25 mL MeCN under nitrogen. 2-PyTuMe (167 mg, 1.00 mmol) was added as a solid. The resulting suspension was stirred under nitrogen for roughly an hour at room temperature. This resulted in a white precipitate. The solvent was removed via filtration, and the solid was washed with diethyl ether. The white solid was dried under a vacuum overnight (208 mg, 62.8% yield).

2.3.1.2.3 Synthesis of $(CuBr)_2(3\text{-PyTuPh})_3$•acetone

Copper(I) bromide (143 mg, 1.00 mmol) was dissolved in 25 mL MeCN under nitrogen. 3-PyTuPh (229 mg, 1.00 mmol) was added in acetone solution. The resulting suspension was stirred under nitrogen for roughly an hour at room temperature. This resulted in a bright yellow precipitate. The solvent was removed via filtration, and the solid was washed with diethyl ether. The bright yellow solid was dried under a vacuum overnight (316 mg, 91.9% yield).

2.3.1.2.4 Synthesis of CuBr(3-PyTuMe)

Copper(I) bromide (143 mg, 1.00 mmol) was dissolved in 25 mL MeCN under nitrogen. 3-PyTuMe (167 mg, 1.00 mmol) was added as a solid. The resulting suspension was stirred under nitrogen for roughly an hour at room temperature. This resulted in a white precipitate. The solvent was removed via filtration, and the solid was washed with diethyl ether. The white solid was dried under a vacuum overnight (221 mg, 62.9% yield).

2.3.1.2.5 Synthesis of CuBr(4-PyTuPh)

Copper(I) bromide (287 mg, 2.00 mmol) was dissolved in 20 mL MeCN under nitrogen. 4-PyTuPh (459 mg, 2.00 mmol) was suspended in 15 mL MeCN and injected into the CuBr solution. The resulting suspension was stirred under nitrogen for roughly an hour at room temperature. This resulted in a green precipitate. The solvent was removed via filtration, and the solid was washed with diethyl ether. The pale green solid was dried under a vacuum overnight (364 mg, 48.4% yield).

2.3.1.2.6 Synthesis of CuBr(PymTuPh)

Copper(I) bromide (143 mg, 1.00 mmol) was dissolved in 25 mL MeCN under nitrogen. PymTuPh (229 mg, 1.00 mmol) was added as a solid. The resulting suspension was stirred under nitrogen for roughly an hour at room temperature. This resulted in a white precipitate. The solvent was removed via filtration, and the solid was washed with diethyl ether. The white solid was dried under a vacuum overnight (318 mg, 85.4% yield).

2.3.1.2.7 Synthesis of CuBr(PymTuMe)

Copper(I) bromide (143 mg, 1.00 mmol) was dissolved in 25 mL MeCN under nitrogen. PymTuMe (167 mg, 1.00 mmol) was added as a solid. The resulting suspension was stirred under nitrogen for roughly an hour at room temperature. This resulted in a white precipitate. The solvent was removed via filtration, and the solid was washed with diethyl ether. The white solid was dried under a vacuum overnight (244 mg, 78.5% yield).

2.3.1.2.8 Synthesis of CuBr(BztTuMe)

Copper(I) bromide (143 mg, 1.00 mmol) was dissolved in 25 mL MeCN under nitrogen. BztTuMe (223 mg, 1.00 mmol) was added as a solid. The resulting suspension was stirred under nitrogen for roughly an hour at room temperature. This resulted in a yellow-green precipitate. The solvent was removed via filtration, and the solid was washed with diethyl ether. The yellow-green solid was dried under a vacuum overnight (264 mg, 72.0% yield).

2.3.1.2.9 Synthesis of $(CuBr)_2(ThzTuMe)_3$

Copper(I) bromide (287 mg, 2.00 mmol) was dissolved in 20 mL MeCN under nitrogen. ThzTuMe (347 mg, 2.00 mmol) was suspended in 15 mL MeCN and injected into the CuBr solution. The resulting suspension was stirred under nitrogen for roughly an hour at room temperature. This resulted in a white precipitate. The solvent was removed via filtration, and the solid was washed with diethyl ether. The white solid was dried under a vacuum overnight (433 mg, 80.5% yield).

2.3.1.2.10 Synthesis of $CuBr[(2\text{-}Py)_2Tu]$

Copper(I) bromide (287 mg, 2.00 mmol) was dissolved in 20 mL MeCN under nitrogen. $(2\text{-}Py)_2Tu$ (461 mg, 2.00 mmol) was suspended in 15 mL MeCN and injected into the CuBr solution. The resulting suspension was stirred under nitrogen for roughly an hour at room temperature. This resulted in a yellow precipitate. The solvent was removed via filtration, and the solid was washed with diethyl ether. The yellow solid was dried under a vacuum overnight (596 mg, 79.7% yield).

2.3.1.2.11 Synthesis of $CuBr[(3\text{-}Py)_2Tu]_5$

Copper(I) bromide (287 mg, 2.00 mmol) was dissolved in 20 mL MeCN under nitrogen. $(3\text{-}Py)_2Tu$ (461 mg, 2.00 mmol) was suspended in 15 mL MeCN and injected

into the CuBr solution. The resulting suspension was stirred under nitrogen for roughly an hour at room temperature. This resulted in a gray precipitate. The solvent was removed via filtration, and the solid was washed with diethyl ether. The grayish white solid was dried under a vacuum overnight (470 mg, 90.7% yield).

2.3.1.3 Preparation of CuI Complexes

2.3.1.3.1 Synthesis of CuI(2-PyTuPh)

Copper(I) iodide (190 mg, 1.00 mmol) was dissolved in 25 mL MeCN under nitrogen. 2-PyTuPh (229 mg, 1.00 mmol) was added as a solid. The resulting suspension was stirred under nitrogen for roughly an hour at room temperature. This resulted in a white precipitate. The solvent was removed via filtration, and the solid was washed with diethyl ether. The white solid was dried under a vacuum overnight (396 mg, 94.5% yield).

2.3.1.3.2 Synthesis of CuI(2-PyTuMe)•MeCN

Copper(I) iodide (190 mg, 1.00 mmol) was dissolved in 25 mL MeCN under nitrogen. 2-PyTuMe (167 mg, 1.00 mmol) was added as a solid. The resulting suspension was stirred under nitrogen for roughly an hour at room temperature. This resulted in a white precipitate. The solvent was removed via filtration, and the solid was washed with diethyl ether. The white solid was dried under a vacuum overnight (351 mg, 88.2% yield).

2.3.1.3.3 Synthesis of CuI(3-PyTuPh)

Copper(I) iodide (190 mg, 1.00 mmol) was dissolved in 25 mL MeCN under nitrogen. 3-PyTuPh (229 mg, 1.00 mmol) was added as a solid. The resulting suspension

was stirred under nitrogen for roughly an hour at room temperature. This resulted in a yellow-green precipitate. The solvent was removed via filtration, and the solid was washed with diethyl ether. The yellow-green solid was dried under a vacuum overnight (283 mg, 86.2% yield).

2.3.1.3.4 Synthesis of CuI(3-PyTuMe)

Copper(I) iodide (190 mg, 1.00 mmol) was dissolved in 25 mL MeCN under nitrogen. 3-PyTuMe (167 mg, 1.00 mmol) was added as a solid. The resulting suspension was stirred under nitrogen for roughly an hour at room temperature. This resulted in a white precipitate. The solvent was removed via filtration, and the solid was washed with diethyl ether. The white solid was dried under a vacuum overnight (336 mg, 94.1% yield).

2.3.1.3.5 Synthesis of CuI(4-PyTuPh)

Copper(I) iodide (381 mg, 2.00 mmol) was dissolved in 20 mL MeCN under nitrogen. 4-PyTuPh (459 mg, 2.00 mmol) was suspended in 15 mL MeCN and injected into the CuI solution. The resulting suspension was stirred under nitrogen for roughly an hour at room temperature. This resulted in a yellow precipitate. The solvent was removed via filtration, and the solid was washed with diethyl ether. The yellow solid was dried under a vacuum overnight (691 mg, 82.3% yield).

2.3.1.3.6 Synthesis of CuI(PymTuPh)

Copper(I) iodide (190 mg, 1.00 mmol) was dissolved in 25 mL MeCN under nitrogen. PymTuPh (229 mg, 1.00 mmol) was added as a solid. The resulting suspension was stirred under nitrogen for roughly an hour at room temperature. This resulted in a yellow precipitate. The solvent was removed via filtration, and the solid was washed

with diethyl ether. The yellow solid was dried under a vacuum overnight (228 mg, 54.2% yield).

2.3.1.3.7 Synthesis of $(CuI)_2(PymTuMe)_2$

Copper(I) iodide (190 mg, 1.00 mmol) was dissolved in 25 mL MeCN under nitrogen. PymTuMe (167 mg, 1.00 mmol) was added as a solid. The resulting suspension was stirred under nitrogen for roughly an hour at room temperature. This resulted in a yellow precipitate. The solvent was removed via filtration, and the solid was washed with diethyl ether. The yellow solid was dried under a vacuum overnight (349 mg, 97.5% yield).

2.3.1.3.8 Synthesis of $(CuI)_2(BztTuMe)_3$

Copper(I) iodide (190 mg, 1.00 mmol) was dissolved in 25 mL MeCN under nitrogen. BztTuMe (223 mg, 1.00 mmol) was added as a solid. The resulting suspension was stirred under nitrogen for roughly an hour at room temperature. This resulted in a yellow precipitate. The solvent was removed via filtration, and the solid was washed with diethyl ether. The yellow solid was dried under a vacuum overnight (311 mg, 88.8% yield).

2.3.1.3.9 Synthesis of CuI(ThzTuMe)

Copper(I) iodide (381 mg, 2.00 mmol) was dissolved in 20 mL MeCN under nitrogen. ThzTuMe (347 mg, 2.00 mmol) was suspended in 15 mL MeCN and injected into the CuI solution. The resulting suspension was stirred under nitrogen for roughly an hour at room temperature. This resulted in a yellow precipitate. The solvent was removed via filtration, and the solid was washed with diethyl ether. The yellow solid was dried under a vacuum overnight (499 mg, 68.6% yield).

2.3.1.3.10 Synthesis of CuI[(2-Py)$_2$Tu]

Copper(I) iodide (381 mg, 2.00 mmol) was dissolved in 20 mL MeCN under nitrogen. (2-Py)$_2$Tu (461 mg, 2.00 mmol) was suspended in 15 mL MeCN and injected into the CuI solution. The resulting suspension was stirred under nitrogen for roughly an hour at room temperature. This resulted in a yellow precipitate. The solvent was removed via filtration, and the solid was washed with diethyl ether. The yellow solid was dried under a vacuum overnight (665 mg, 79.0% yield).

2.3.1.3.11 Synthesis of CuI[(3-Py)$_2$Tu]$_4$

Copper(I) iodide (381 mg, 2.00 mmol) was dissolved in 20 mL MeCN under nitrogen. (3-Py)$_2$Tu (461 mg, 2.00 mmol) was suspended in 15 mL MeCN and injected into the CuI solution. The resulting suspension was stirred under nitrogen for roughly an hour at room temperature. This resulted in a yellow white precipitate. The solvent was removed via filtration, and the solid was washed with diethyl ether. The yellow white solid was dried under a vacuum overnight (461 mg, 82.9% yield).

2.3.1.4 Preparation of CuNO$_3$ Complexes

2.3.1.4.1 Synthesis of (CuNO$_3$)$_2$(2-PyTuPh)$_3$

Cu(NO$_3$)$_2$•2.5H$_2$O (233 mg, 1.00 mmol) and excess copper wool were stirred at room temp. in 25 mL MeCN until the blue color discharged. 2-PyTuPh (229 mg, 1.00 mmol) was added as a solid. The resulting suspension was stirred under nitrogen for roughly an hour at room temperature. This resulted in a brown precipitate. The solvent was removed via filtration, and the solid was washed with diethyl ether. The light brown solid was dried under a vacuum overnight (≈300 mg, ≈95% yield).

2.3.1.4.2 Synthesis of $CuNO_3$(2-PyTuMe)•MeCN

$Cu(NO_3)_2$•$2.5H_2O$ (233 mg, 1.00 mmol) and excess copper wool were stirred at room temp. in 25 mL MeCN until the blue color discharged. 2-PyTuMe (167 mg, 1.00 mmol) was added as a solid. The resulting suspension was stirred under nitrogen for roughly an hour at room temperature. This resulted in a white precipitate. The solvent was removed via filtration, and the solid was washed with diethyl ether. The white solid was dried under a vacuum overnight (211 mg, 89.2% yield).

2.3.1.4.3 Synthesis of $CuNO_3$(3-PyTuPh)•1.5acetone

$Cu(NO_3)_2$•$2.5H_2O$ (233 mg, 1.00 mmol) and excess copper wool were stirred at room temp. in 25 mL MeCN until the blue color discharged. 3-PyTuPh (229 mg, 1.00 mmol) was added as a solution in acetone. The resulting suspension was stirred under nitrogen for roughly an hour at room temperature. This resulted in a yellow precipitate. The solvent was removed via filtration, and the solid was washed with diethyl ether. The yellow solid was dried under a vacuum overnight (358 mg, 90.4% yield).

2.3.1.4.4 Synthesis of $CuNO_3$(3-PyTuMe)•2MeCN

$Cu(NO_3)_2$•$2.5H_2O$ (233 mg, 1.00 mmol) and excess copper wool were stirred at room temp. in 25 mL MeCN until the blue color discharged. 3-PyTuMe (167 mg, 1.00 mmol) was added as a solid. The resulting suspension was stirred under nitrogen for roughly an hour at room temperature. This resulted in an off-white precipitate. The solvent was removed via filtration, and the solid was washed with diethyl ether. The off-white solid was dried under a vacuum overnight (301 mg, 80.2% yield).

2.3.1.4.5 Synthesis of $(CuNO_3)_2$(4-PyTuPh)$_3$

$Cu(NO_3)_2 \cdot 2.5H_2O$ (233 mg, 1.00 mmol) and excess copper wool were stirred at room temp. in 20 mL MeCN until the blue color discharged. 4-PyTuPh (459 mg, 2.00 mmol) was suspended in 15 mL MeCN and injected into the $Cu(I)NO_3$ solution. The resulting suspension was stirred under nitrogen for roughly an hour at room temperature. This resulted in a yellow precipitate. The solvent was removed via filtration, and the solid was washed with diethyl ether. The yellow solid was dried under a vacuum overnight (402 mg, 41.8% yield).

2.3.1.4.6 Synthesis of $CuNO_3$(PymTuPh)

$Cu(NO_3)_2 \cdot 2.5H_2O$ (233 mg, 1.00 mmol) and excess copper wool were stirred at room temp. in 15 mL MeCN until the blue color discharged. PymTuPh (461 mg, 2.00 mmol) was added as a solid. The resulting suspension was stirred under nitrogen for roughly an hour at room temperature. This resulted in a yellow precipitate. The solvent was removed via filtration, and the solid was washed with diethyl ether. The yellow solid was dried under a vacuum overnight (234 mg, 53.1% yield).

2.3.1.4.7 Synthesis of $(CuNO_3)_2$(PymTuMe)$_3$

$Cu(NO_3)_2 \cdot 2.5H_2O$ (233 mg, 1.00 mmol) and excess copper wool were stirred at room temp. in 25 mL MeCN until the blue color discharged. PymTuMe (167 mg, 1.00 mmol) was added as a solid. The resulting suspension was stirred under nitrogen for roughly an hour at room temperature. This resulted in a yellow precipitate. The solvent was removed via filtration, and the solid was washed with diethyl ether. The yellow solid was dried under a vacuum overnight (179 mg, 71.4% yield).

2.3.1.4.8 Synthesis of $CuNO_3$(BztTuMe)•MeCN

$Cu(NO_3)_2$•$2.5H_2O$ (233 mg, 1.00 mmol) and excess copper wool were stirred at room temp. in 25 mL MeCN until the blue color discharged. BztTuMe (223 mg, 1.00 mmol) was added as a solid. This suspension was stirred under nitrogen for roughly an hour at room temperature. This resulted in a light green precipitate. The solvent was removed via filtration, and the solid was washed with diethyl ether. The light green solid was dried under a vacuum overnight (221 mg, 63.4% yield).

2.3.1.4.9 Synthesis of $CuNO_3(ThzTuMe)_2$

$Cu(NO_3)_2$•$2.5H_2O$ (233 mg, 1.00 mmol) and excess copper wool were stirred at room temp. in 20 mL MeCN until the blue color discharged. ThzTuMe (459 mg, 2.00 mmol) was suspended in 15 mL MeCN and injected into the $CuNO_3$ solution. The resulting suspension was stirred under nitrogen for roughly an hour at room temperature. This resulted in a brown precipitate. The solvent was removed via filtration, and the solid was washed with diethyl ether. The light brown solid was dried under a vacuum overnight (60 mg, 7.4% yield).

2.3.1.4.10 Synthesis of $(CuNO_3)_2[(2\text{-}Py)_2Tu]_3$•MeCN (1 hr. time scale)

$Cu(NO_3)_2$•$2.5H_2O$ (233 mg, 1.00 mmol) and excess copper wool were stirred at room temp. in 20 mL MeCN until the blue color discharged. $(2\text{-}Py)_2Tu$ (461 mg, 2.00 mmol) was suspended in 15 mL MeCN and injected into the $CuNO_3$. The resulting suspension was stirred under nitrogen for roughly an hour at room temperature. This resulted in a yellow precipitate. The solvent was removed via filtration, and the solid was washed with diethyl ether. The yellow solid was dried under a vacuum overnight (487 mg, 24.8% yield).

2.3.1.4.11 Synthesis of $CuNO_3[(2\text{-}Py)_2Tu]_2$ (4 hr. time scale)

$Cu(NO_3)_2 \cdot 2.5H_2O$ (233 mg, 1.00 mmol) and excess copper wool were stirred at room temp. in 20 mL MeCN until the blue color discharged. $(2\text{-}Py)_2Tu$ (461 mg, 2.00 mmol) was suspended in 15 mL MeCN and injected into the $Cu(I)NO_3$ solution. The resulting suspension was stirred under nitrogen for roughly four hours at room temperature. This resulted in an orange precipitate. The solvent was removed via filtration, and the solid was washed with diethyl ether. The orange solid was dried under a vacuum overnight (528 mg, 45.0% yield).

2.3.1.4.12 Synthesis of $CuNO_3[(3\text{-}Py)_2Tu] \cdot MeCN$

$Cu(NO_3)_2 \cdot 2.5H_2O$ (233 mg, 1.00 mmol) and excess copper wool were stirred at room temp. in 20 mL MeCN until the blue color discharged. $(3\text{-}Py)_2Tu$ (461 mg, 2.00 mmol) was suspended in 15 mL MeCN and injected into the $Cu(I)NO_3$ solution. The resulting suspension was stirred under nitrogen for roughly an hour at room temperature. This resulted in a yellow precipitate. The solvent was removed via filtration, and the solid was washed with diethyl ether. The yellow solid was dried under a vacuum overnight (638 mg, 80.4% yield).

2.3.2 X-ray diffraction studies

Crystals were grown in 5 mm tubes by two techniques. Generally, CuX (X = Cl^-, Br^-, I^-, or NO_3^-) was dissolved in acetonitrile and layered with a thiourea dissolved in acetonitrile (MeCN). In cases where the thiourea was insoluble in MeCN, acetone was used to dissolve the thiourea that was then layered over the CuX compound dissolved in MeCN. Also, in cases for which the reaction occurred sufficiently slowly to grow useful crystals without relying on a slow mixing, CuX and the thiourea were combined before

addition to the crystal tube, and layered with ether. Single crystal determinations were carried out using a Bruker *SMART Apex II* diffractometer at 100 K using graphite-monochromated Cu Kα radiation. The data were corrected for Lorentz and polarization effects and absorption using *SADABS* [19]. The structures were solved by use of direct methods or Patterson map. Least squares refinement on F^2 was used for all reflections. Structure solution, refinement and the calculation of derived results were performed using the *SHELXTL* [20] package of software. The non-hydrogen atoms were refined anisotropically. In all cases, hydrogen atoms were located then placed in theoretical positions. Selected bond lengths for all copper(I) thiourea complexes whose crystal structures were solved are provided in Table **5**. Selected bond angles around copper atom for these complexes are provided in Table **6**.

3 Results and Discussion

3.1 Heterocyclic Thioureas

The then heterocyclic-substituted thioureas, **1**–**10** are shown below.

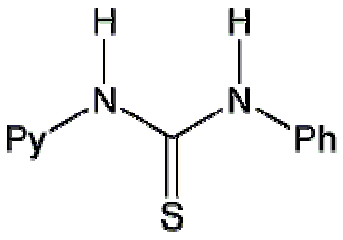

Py = 3-pyridyl, **1**; 4-pyridyl, **2**

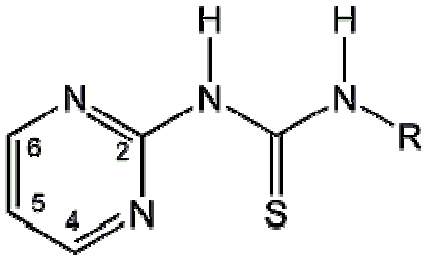

R = Ph, **3**; CH_3, **4**

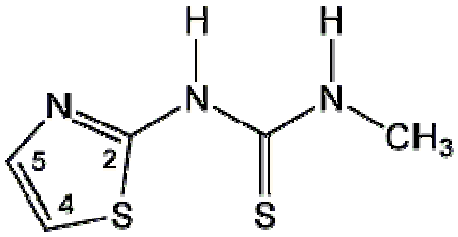

5

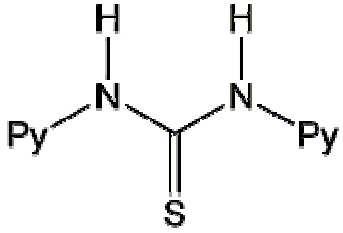

Py = 2-pyridyl, **6**; 3-pyridyl, **7**

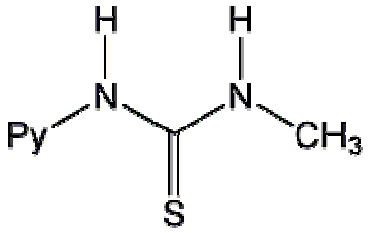

Py = 3-pyridyl, **8**; 2-pyridyl, **9**

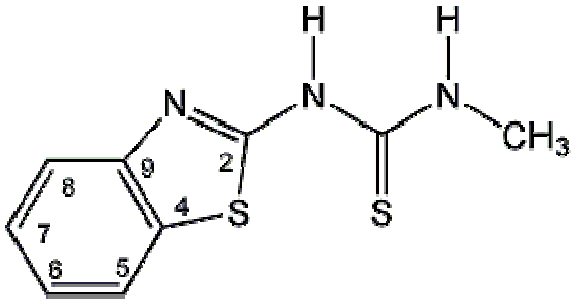

10

were synthesized through the reactions of phenyl- or methylisothiocyanate with various aminoheterocycles ($ArNH_2$) according to reaction (1) [2, 8, 22-24]. In all cases, good yields were realized. The two homo-substituted thioureas, **6** and **7** were produced by the

reaction of aminopyridines with carbon disulfide in pyridine according to reactions (2a) and (2b) [24, 25]. While 2- and 3-aminopyridine produced compounds **6** and **7**, the attempted reaction with 4-aminopyridine produced a yellow solid that was provisionally identified based upon NMR data as 4-aminopyridinium *N*-(4-pyridyl)dithiocarbamate [23]. Thus, reaction (3) failed to occur presumably due to relatively weak nucleophilicity of 4-aminopyridine.

$$ArNH_2 + RN{=}C{=}S \rightarrow ArNHC(=S)NHR \quad (1)$$

$$PyNH_2 + CS_2 \rightarrow PyNHC(=S)SH \quad (2a)$$

$$PyNH_2 + PyNHC(=S)SH \rightarrow (PyNH)_2C{=}S + H_2S \quad (2b)$$

Thioureas **8, 9,** and **10** did not grow crystals and so were unable to be characterized by X-ray crystallography.

3.1.1 X-Ray Crystallography

Crystal growth techniques for thioureas have been discussed previously in Section 2.2.2. X-ray quality crystals were produced for seven thioureas. Table 1 below gives the crystal and structure refinement data for all seven crystals.

Table 1 Crystal and structure refinement data[a]

	1	2	3	4	5	6	7
CCDC deposit no.	655874	655878	655875	655879	655877	655876	655880
Color and habit	colorless needle	colorless block	colorless block	colorless plate	colorless plate	colorless block	colorless plate
Size, mm	0.41 × 0.04 × 0.04	0.41 × 0.28 × 0.23	0.43 × 0.28 × 0.27	0.21 × 0.20 × 0.05	0.19 × 0.18 × 0.06	0.51 × 0.43 × 0.30	0.25 × 0.08 × 0.02
Formula	$C_{12}H_{11}N_3S$	$C_{12}H_{11}N_3S$	$C_{11}H_{10}N_4S$	$C_6H_8N_4S$	$C_5H_7N_3S_2$	$C_{11}H_{10}N_4S$	$C_{11}H_{10}N_4S$
Formula weight	229.30	229.30	230.29	168.22	173.26	230.29	230.29
Space group	$Pna2_1$ (#33)	$P2_1/c$ (#14)	$P2_1/c$ (#14)	$P2_1/c$ (#14)	$C2/c$ (#15)	$Fdd2$ (#43)	$P2_1/c$ (#14)
a (Å)	10.1453(3)	16.9314(3)	5.45900(10)	8.8159(5)	17.9308(3)	15.1859(2)	13.2461(2)
b (Å)	17.6183(5)	10.3554(2)	13.8559(2)	11.2386(5)	7.78260(10)	30.1654(3)	6.26170(10)
c (Å)	6.4787(2)	13.5152(3)	14.3356(3)	7.7156(4)	10.8686(2)	9.44130(10)	12.3503(2)
β (deg)	90	106.5080(10)	94.9800(10)	95.629(2)	105.3740(10)	90	96.0160(10)
Volume ($Å^3$)	1158.02(6)	2271.96(8)	1080.24(3)	760.76(7)	1462.42(4)	4324.95(8)	1018.73(3)
Z	4	8	4	4	8	16	4
ϱ_{calc} (g cm^{-3})	1.315	1.341	1.416	1.469	1.574	1.415	1.501
F_{000}	480	960	480	352	720	1920	480
μ (Cu Kα) (mm^{-1})	2.271	2.315	2.465	3.263	5.970	2.463	2.614
Radiation	CuKα (λ = 1.54178 Å)	CuKα (λ = 1.54178 Å)	CuKα (λ = 1.54178 Å)	CuKα (λ = 1.54178 Å)	CuKα (λ = 1.54178 Å)	CuKα (λ = 1.54178 Å)	CuKα (λ = 1.54178 Å)
Temperature (K)	200	100	100	100	100	100	100
Residuals:[a] R; R_w	0.0276; 0.0544	0.0285; 0.0722	0.0297; 0.0839	0.0255; 0.0731	0.0232; 0.0620	0.0194; 0.0512	0.0266; 0.0714
Goodness of fit	1.081	1.088	1.030	1.046	1.054	1.029	1.022

[a] $R = R_1 = \Sigma||F_o|-|F_c||/(\Sigma|F_o|$ for observed data only. $R_w = wR_2 = \{\Sigma[w(F_o^2-F_c^2)^2]/\Sigma[w(F_o^2)^2]\}^{1/2}$ for all data

Selected bond distances (Å) and angles (°)[a] for all seven thioureas are listed in Table 2

Table 2 Selected bond distances (Å) and angles (°)[a]

	1	2	3	4	5	6	7
C1–S1	1.6990(19)	1.6950(14), 1.6985(14)	1.6813(14)	1.6858(13)	1.6932(15)	1.6736(13)	1.6763(14)
C1–N1	1.332(3)	1.3505(18), 1.3565(17)	1.3807(17)	1.3878(16)	1.375(2)	1.3501(16)	1.3644(18)
C1–N2	1.344(2)	1.3481(18), 1.3375(18)	1.3350(18)	1.3181(17)	1.325(2)	1.3737(16)	1.3654(18)
N1–C2	1.435(2)	1.4144(18), 1.4101(17)	1.3900(18)	1.3842(16)	1.379(2)	1.4010(15)	1.4175(18)
N2–CX	1.424(2)	1.4234(18), 1.4301(18)	1.4264(17)	1.4557(16)	1.452(2)	1.4045(18)	1.4123(18)
N1–C1–N2	118.66(18)	117.30(12), 116.68(12)	116.66(12)	117.40(11)	117.14(13)	114.59(12)	111.55(12)
N1–C1–S1	121.96(15)	123.11(10), 123.60(10)	119.57(10)	118.66(9)	119.00(11)	126.99(10)	124.52(11)
N2–C1–S1	119.36(15)	119.54(10), 119.69(10)	123.76(10)	123.94(9)	123.86(12)	118.42(9)	123.93(11)
C2–N1–C1	122.11(16)	125.48(12), 125.21(12)	129.64(12)	129.54(11)	127.09(13)	131.16(12)	124.41(13)
CX–N2–C1	127.85(19)	129.43(12), 128.30(12)	125.36(12)	124.06(11)	123.57(14)	130.69(11)	123.73(12)

[a] CX = C7 for **1**, **2**, **6**, and **7**; C6 for **3** and **4**; C5 for **5**

Selected Hydrogen-bond distances (Å) and angles (°) are listed in Table 3.

Table 3 Hydrogen-bond distances (Å) and Angles (°)

Compound	D–H···A	H···A dist.	D···A dist.	D–H···A angle
1	N2–H2···S1[a]	2.47(2)	3.329(2)	164.7(19)
	N1–H1···N3[b]	2.14(2)	2.936(2)	159(2)
2	N1–H1N···N6[c]	2.109(19)	2.8305(17)	154.1(17)
	N2–H2N···S1[d]	2.527(19)	3.3434(12)	162.0(16)
	N4–H4N···N3	2.059(19)	2.8498(17)	156.6(16)
	N5–H5N···S2[e]	2.449(19)	3.3274(12)	165.2(15)
3	N1–H1···N4[f]	2.265(19)	3.0824(16)	177.8(16)
	N2–H2···N3	1.926(19)	2.6399(16)	140.7(17)
4	N2–H2N···N3	1.966(19)	2.6578(16)	139.3(18)
	N1–H1N···N4[g]	2.302(17)	3.0943(16)	171.1(13)
5	N1–H1N···S1[h]	2.52(2)	3.3184(14)	169.2(18)
	N2–H2N···N3	2.000(19)	2.6911(18)	140.9(17)
6	N2–H2···N3[i]	2.234(19)	3.0779(14)	170.3(16)
	N1–H1···N4	1.87(2)	2.6534(16)	144.7(18)
7	N2–H2N···N4[j]	2.13(2)	2.9526(18)	167.5(17)
	N1–H1N···N3[k]	2.28(2)	3.0728(18)	163.7(16)

Symmetry transformations used to generate equivalent atoms: [a]$-x, -y + 1, z + 1/2$; [b]$x + 1/2, -y + 1/2, z$; [c]$x,y-1,z$; [d]$-x, -y + 1, -z + 2$; [e]$-x + 1, -y + 2, -z + 1$; [f]$-x + 1, -y + 2, -z + 1$; [g]$-x + 1, -y, -z$; [h]$-x + 2, y, -z + 3/2$; [i]$x + 1/4, -y + 3/4, z-1/4$; [j]$x, -y + 3/2, z-1/2$; [k]$x, y + 1, z$

Interplanar angles (˚) for all seven thioureas are listed in Table 4.

Table 4 Interplanar angles (°)

Compound	Ring 1–ring 2[a]	Ring 1–NC(S)N[a]	Ring 2–NC(S)N[a]
1	51.09(6)	86.22(6)	64.62(6)
2	88.58(5), 82.15(5)	46.09(6), 55.62(4)	58.59(4), 48.87(6)
3	68.48(3)	5.91(6)	66.22(3)
4	–	1.94(6)	–
5	–	5.23(7)	–
6	24.16(6)	20.91(5)	8.03(7)
7	72.21(4)	57.73(4)	56.99(4)

[a] Ring 1 is the heterocyclic ring in **1–5**. Ring 2 is the phenyl in **1–3**

3.1.1.1 (3-Py)TuPh, **1***, (4-Py)TuPh,* **2**

In contrast to the intramolecular H-bonding behavior uniformly encountered for *ortho*-heterocylic thioureas, placement of the pyridine nitrogen at the 3- or 4-position produced only intermolecular hydrogen-bonds, resulting in the formation of extended networks. Compound **1** crystallizes in the non-centrosymmetric orthorhombic space group *P*na2_1 (Flack parameter = 0.022(18)). A molecular diagram is shown in Figure 8 and a packing diagram emphasizing the 3D H-bonding network is shown in Figure 9.

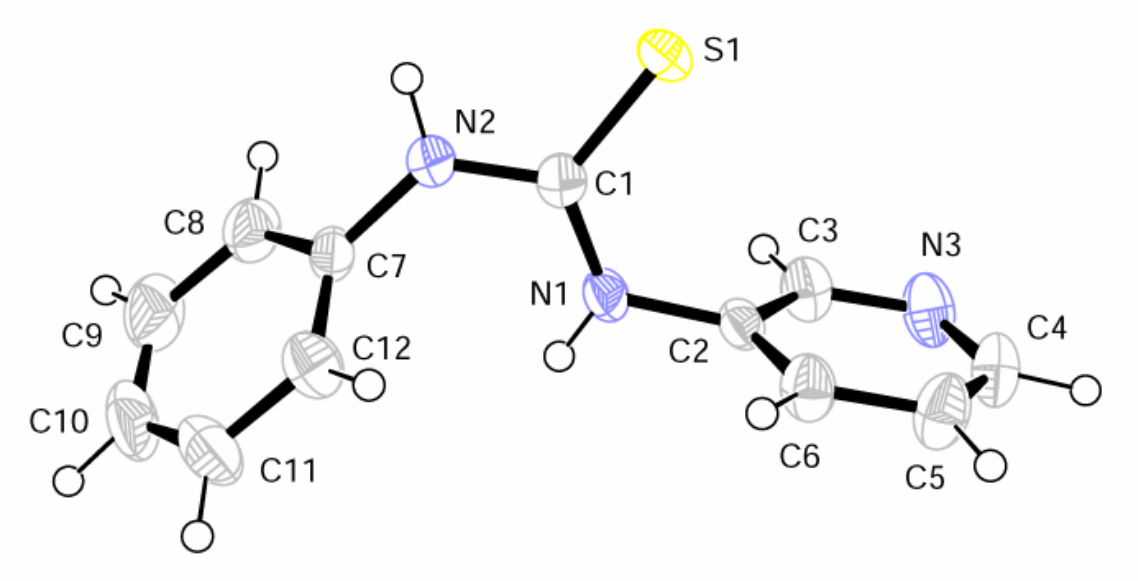

Figure 8: Molecular Structure of **1**.

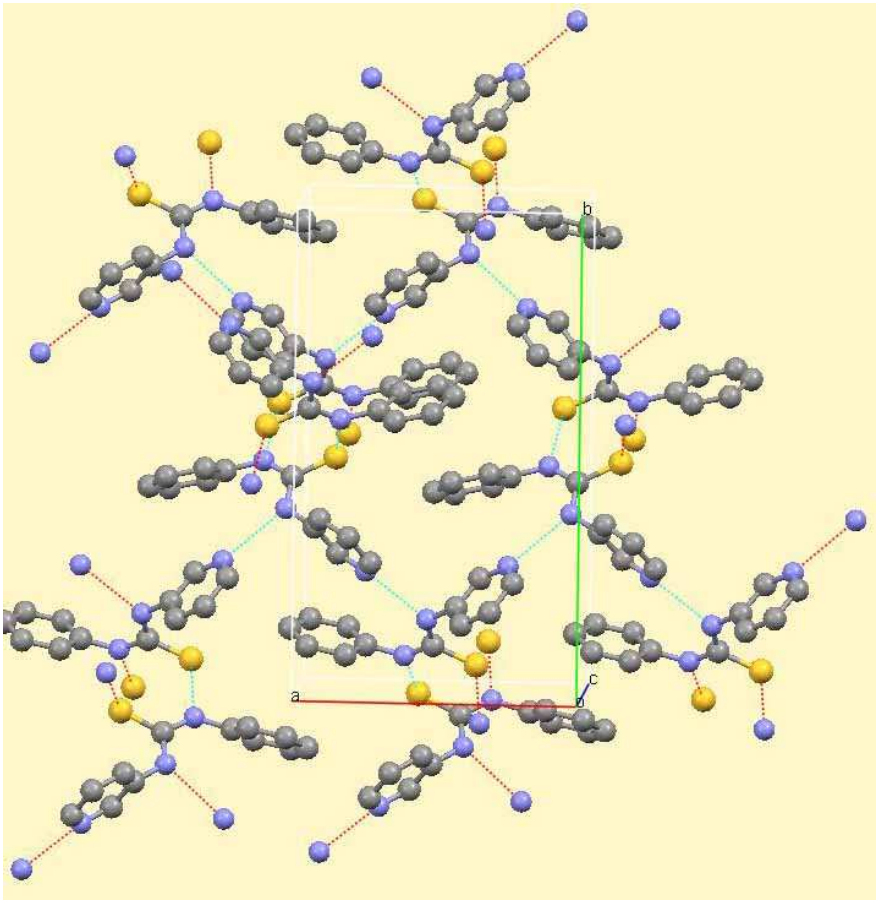

Figure 9: Hydrogen bonding network and packing diagram for **1**.

As is the case with each of the compounds described herein, the molecular structure of **1** is unremarkable. Also, like all but one of the disubstituted thiourea structures reported herein, one thiourea substituent (the phenyl ring) is oriented toward the thiocarbonyl carbon and the other toward the sulfur (EZ conformation).

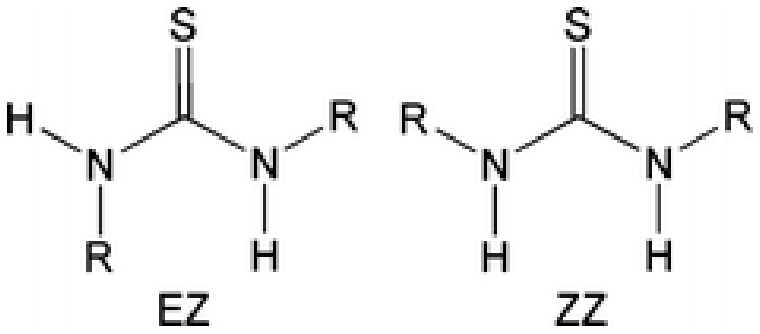

The two ring planes lie at fairly large angles to one another and also to the plane defined by the thiourea core (NC(S)N), see Table 4. The bond lengths and angles within the thiourea core are relatively symmetrical. Two intermolecular H-bonds are seen in **1**: N1–H···N3 (Tu···Py, Tu = thiourea) and N2–H···S1 (Tu···Tu) (see Table 3 for H-bonding distances). The relatively long N···S distances encountered for compounds **1**, **2**, and **5** are facilitated by resonance lengthening of C=S (see Table 2), [10] and are similar to those of previously determined thiourea dimers [3, 5–8]. Helices, consisting of six H-bonded molecules were found to propagate parallel to the *c*-axis forming channels. The phenyl rings lie within these channels. The helices are tiled together with pairs of molecules producing junctions between them. Curiously, the oxygen analog of **1**, *N*-(3-pyridyl)-*N*′-phenylurea reveals a ZZ conformation in the crystal structure and shows no H-bonding [26].

Compound **2** crystallizes in the monoclinic space group $P2_1/c$. A molecular diagram is shown in Figure 10 and a packing diagram with H-bonding emphasized is shown in Figure 11.

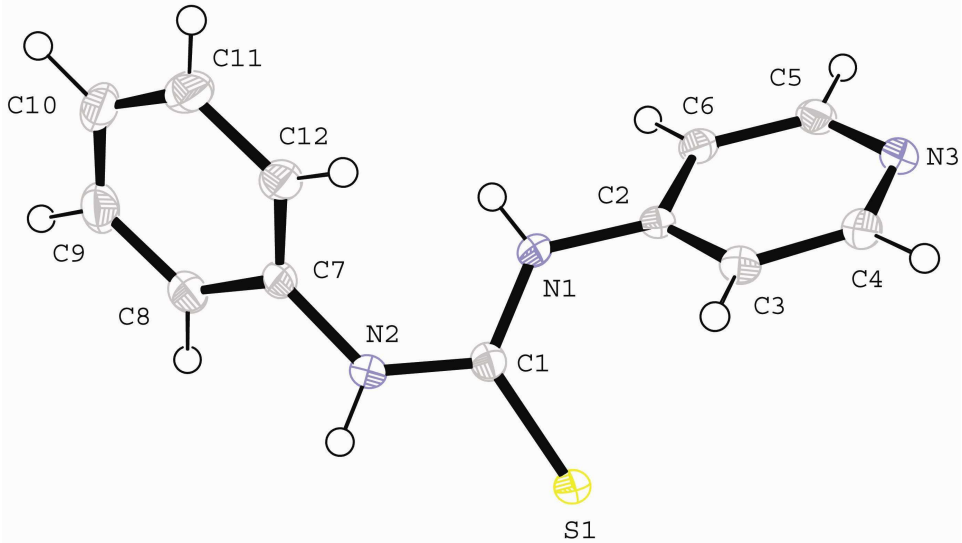

Figure 10: Molecular structure of **2**.

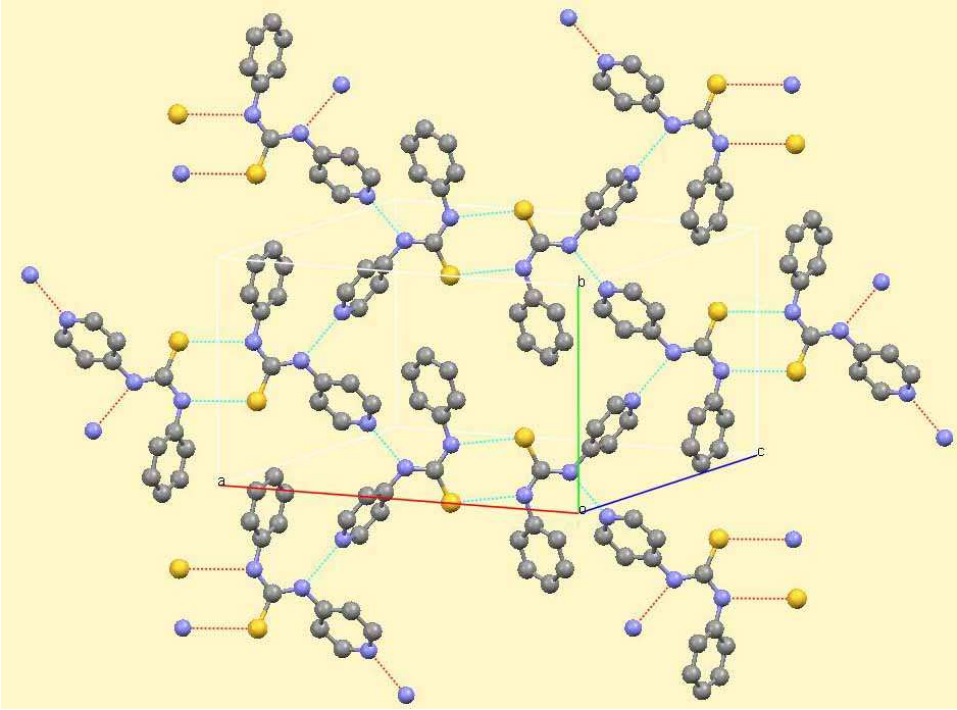

Figure 11: Hydrogen bonding network and packing diagram for **2**. Hydrogen atoms omitted for clarity

Two independent molecules are present in structure. In similar fashion to **1**, compound **2** forms a symmetrical thiourea core with an EZ conformation (pyridyl is oriented toward sulfur in this case) and shows large interplanar angles between the various combinations of the rings and the thiourea core (Table 4). Pairs of intermolecular H-bonds are formed, one pair for each independent molecule: N1–H···N6, N4–H···N3 (Tu···Py) and N2–H···S1, N5–H···S2 (Tu···Tu). All H-bonds are roughly coplanar, producing a flat 2D sheet structure. The sheets are composed of tiled hexagonal rings constructed from six **2** molecules. The sheets run parallel to the crystallographic *b*-axis and the *a*,*c*-diagonal. The analogous urea, N-(4-pyridyl)-N′-phenylurea, exhibits a Z,Z conformation and shows only a single N–H···N (urea···Py) H-bond, resulting in a chain structure [26].

3.1.1.2 PymTuPh **3***, PymTuMe* **4***, ThzTuMe* **5**

Each of these heterocyclic thioureas features an *ortho*-nitrogen. As a result each compound displays an internal H-bond, such as has been seen for related species (see above). Since intramolecular H-bonding requires an E conformation, all three molecules crystallize as EZ conformers. In contrast to most of the known *ortho*-heterocyclic thioureas, **3**–**5** all form H-bonded dimers. Compound **3** crystallizes in $P2_1/c$. The molecular structure of compound 3 is shown in Figure 12. A molecular diagram of the H-bonded dimer, shown in Figure 13, reveals both an internal H-bond, N2–H···N3 (Tu···Pym) and an intermolecular H-bond, N1–H···N4 (Tu···Pym). An analogous dimeric structure is exhibited by **4**, which crystallizes in $P2_1/c$, see Figure 14.

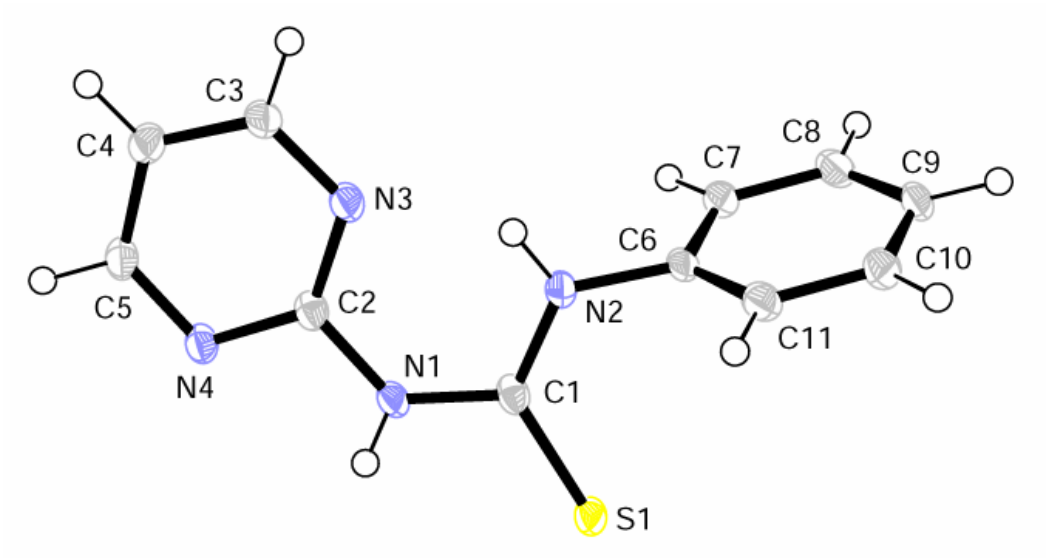

Figure 12: Molecular structure of **3**

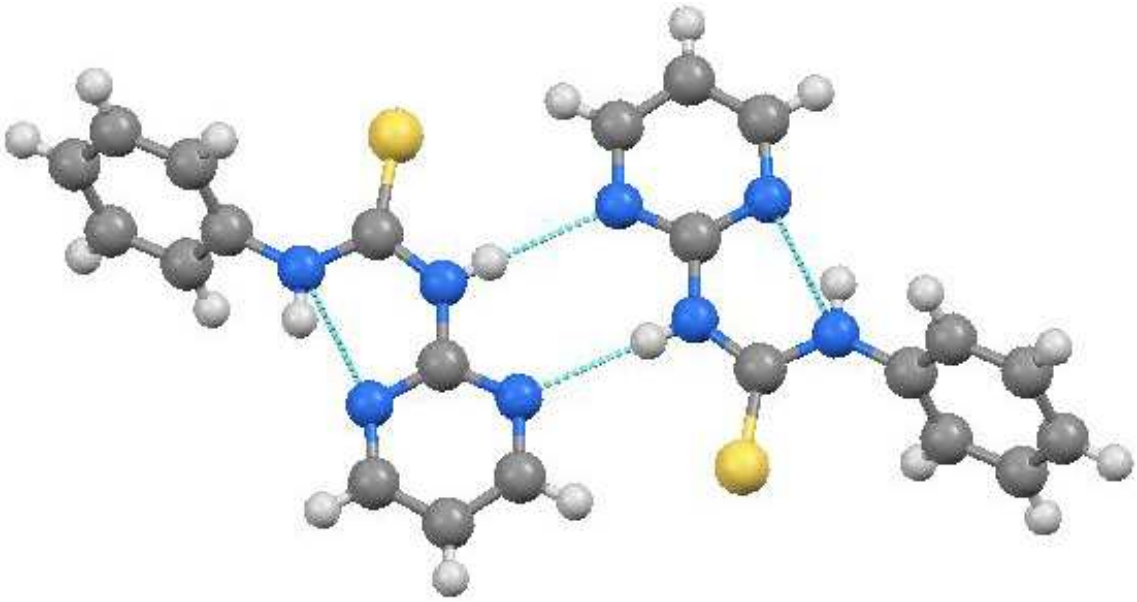

Figure 13: Hydrogen bonding dimer for **3**.

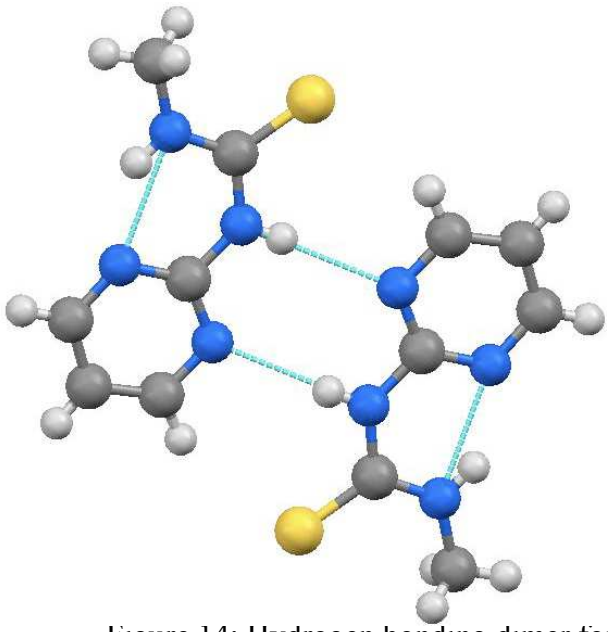

Figure 14: Hydrogen bonding dimer for **4.**

Dimers are also formed by **5**, which crystallizes in the monoclinic space group *C*2/c. However, in contrast to compounds **3** and **4** which form dimers through N–H···N interactions, compound **5** forms dimers through N2–H···S2 (Tu···Tu), see Figure 15.

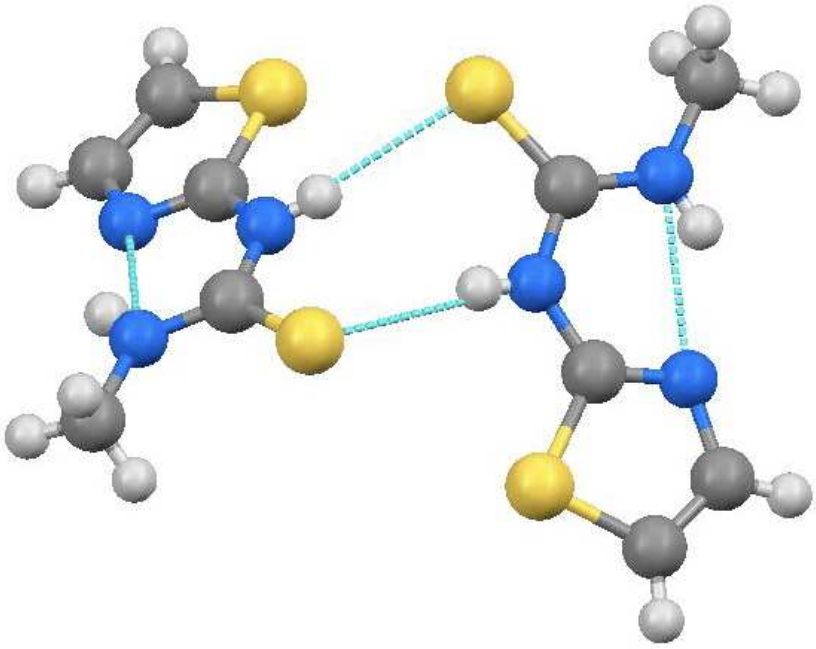

Figure 15: Molecular structure and hydrogen bonding dimer for **5**.

The expected internal N1–H···N3 (Tu···Thz) H-bond is also present. In addition, there is a close interaction between S1 and S2 of 3.6279(5) Å. Compound **5** fails to form H-bonds to either of the thiazole ring heteroatoms. Its dimeric structure is very closely related to that of the known thiazole- and benzothiazole-substituted thioureas, **III** [3, 7].

Compounds **3**–**5** stand apart from the other thioureas reported herein with respect to their core bond lengths. As is revealed by the data in Table 2, pairs of thiourea C1–N1 and C1–N2 bonds are of very different lengths in compounds **3**–**5** (1.375–1.388 vs. 1.318–1.335 Å). In addition, the N1–C2 and N2–CX (CX = C6 for **3** and **4**, CX = C5 for **5**) bonds are inequivalent (1.379–1.390 vs. 1.426–1.456 Å). Finally, it will be noted from the data in Table 4 that the heterocyclic rings in **3**–**5** are nearly coplanar with the thiourea core. These observations, taken together, are almost certainly the result of contributions from resonance forms **3′**–**5′**. Such resonance contributions are facilitated by the presence of an intramolecular H-bond in each compound.

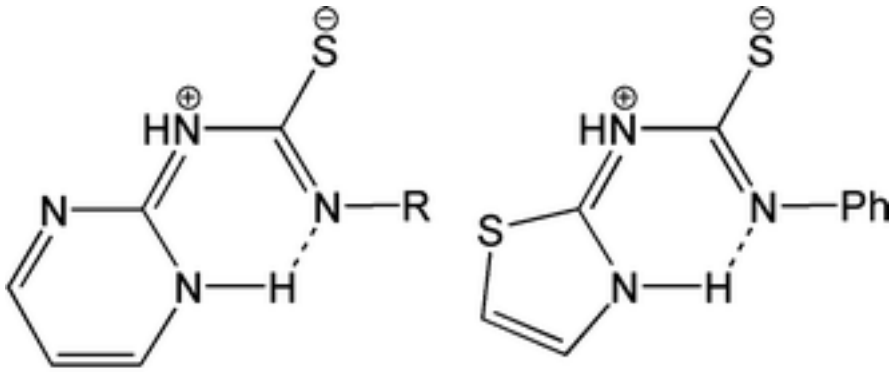

3', R = Ph; **4'**, R = CH_3 **5'**

3.1.1.3 (2-Py)$_2$Tu **6***, (3-Py)$_2$Tu* **7**

These symmetrical dipyridylthioureas both form extended network structures via H-bonding interactions. Compound **6** crystallized in the non-centrosymmetric

orthorhombic space group *F*dd2 (Flack parameter = 0.033(10)). A molecular diagram is shown in Figure 16 and a packing diagram emphasizing the 2D H-bonding network is shown in Figure 17.

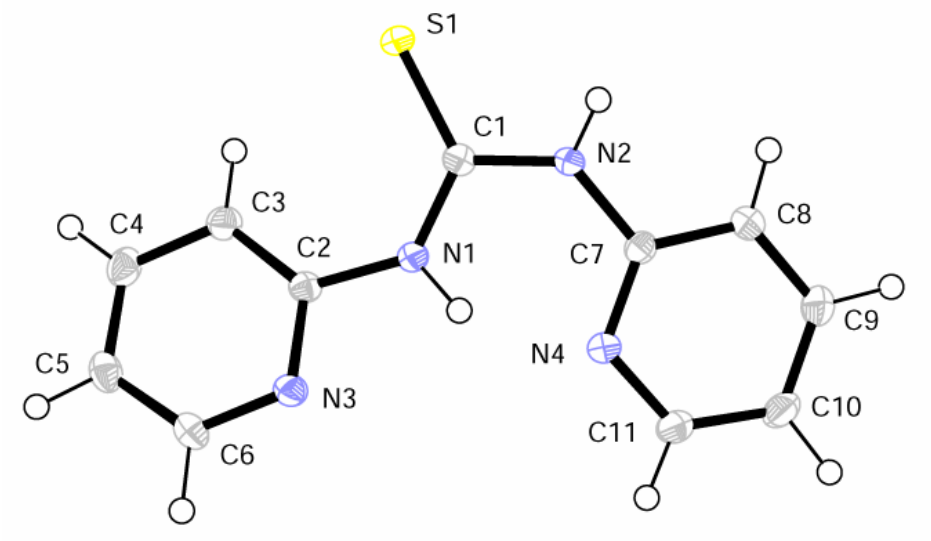

Figure 16: Molecular structure of **6**.

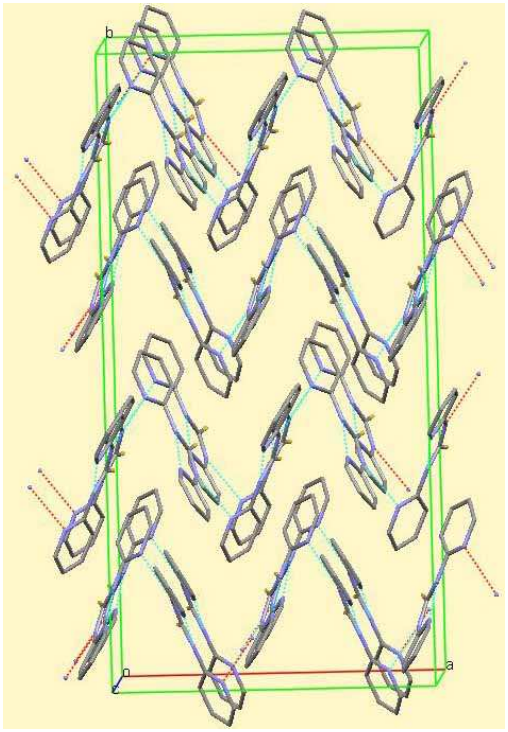

Figure 17: Hydrogen bonding network and packing diagram for **6**. Hydrogen atoms omitted for clarity.

A fairly symmetrical thiourea core is connected to the pyridyl substituents in EZ conformation. Compound **6** shows the expected intramolecular H-bond: N1–H···N4 (Tu···Py). A second, intermolecular, H-bond, N2–H···N3 (Tu···Py) produces a zigzag chain which propagates parallel to the *a*,*c* diagonal. Compound **6** is the only species studied herein that has an *ortho*-substituent on each ring and therefore can form an intramolecular H-bond with either ring. This situation should produce equilibrium between EZ and ZE conformers.

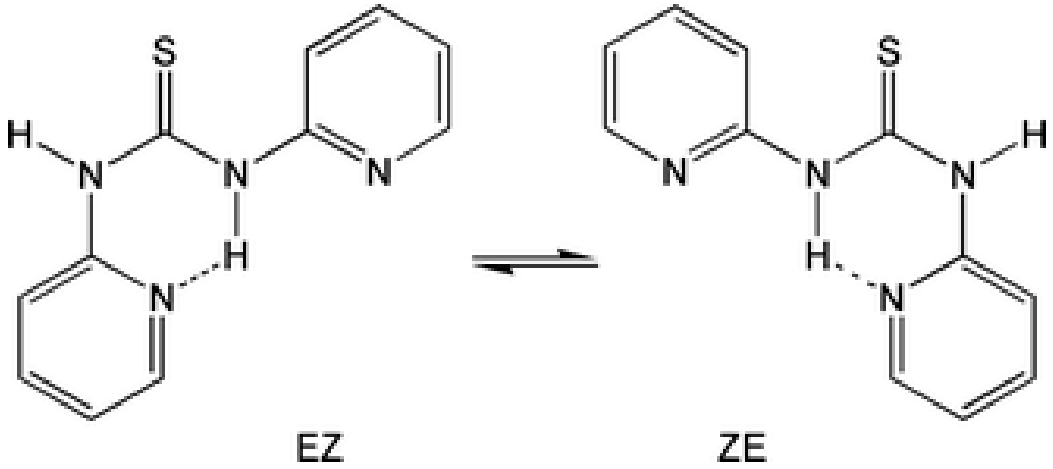

Indeed, the ^{1}H and ^{13}C NMR signals (except for those of the thiocarbonyl and *ipso* ring carbons) are greatly broadened at room temperature, indicating that interchange between the conformers is occurring at an intermediate rate in solution at room temperature.

Compound **7** crystallized in $P2_1/c$, forming a H-bonded sheet which propagates parallel to the *b*,*c*-plane. The molecular diagram for **7**, shown in Figure 18, reveals the only ZZ molecular conformation reported herein. The packing diagram, highlighting H-bonding networking, is shown in Figure 19.

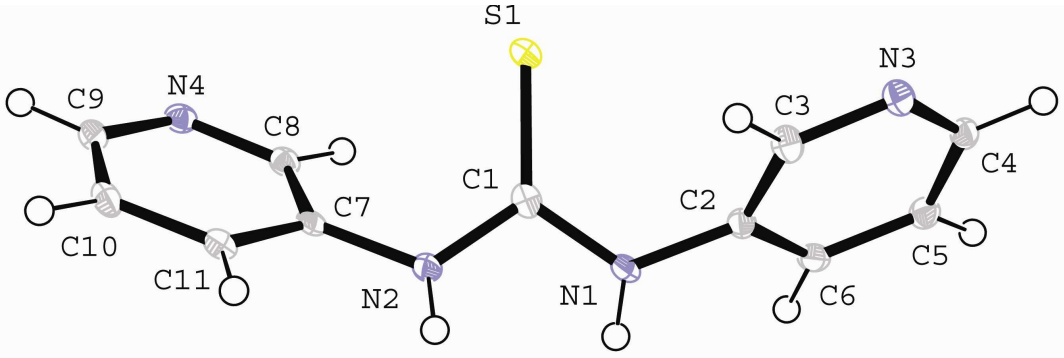

Figure 18: Molecular structure of **7**.

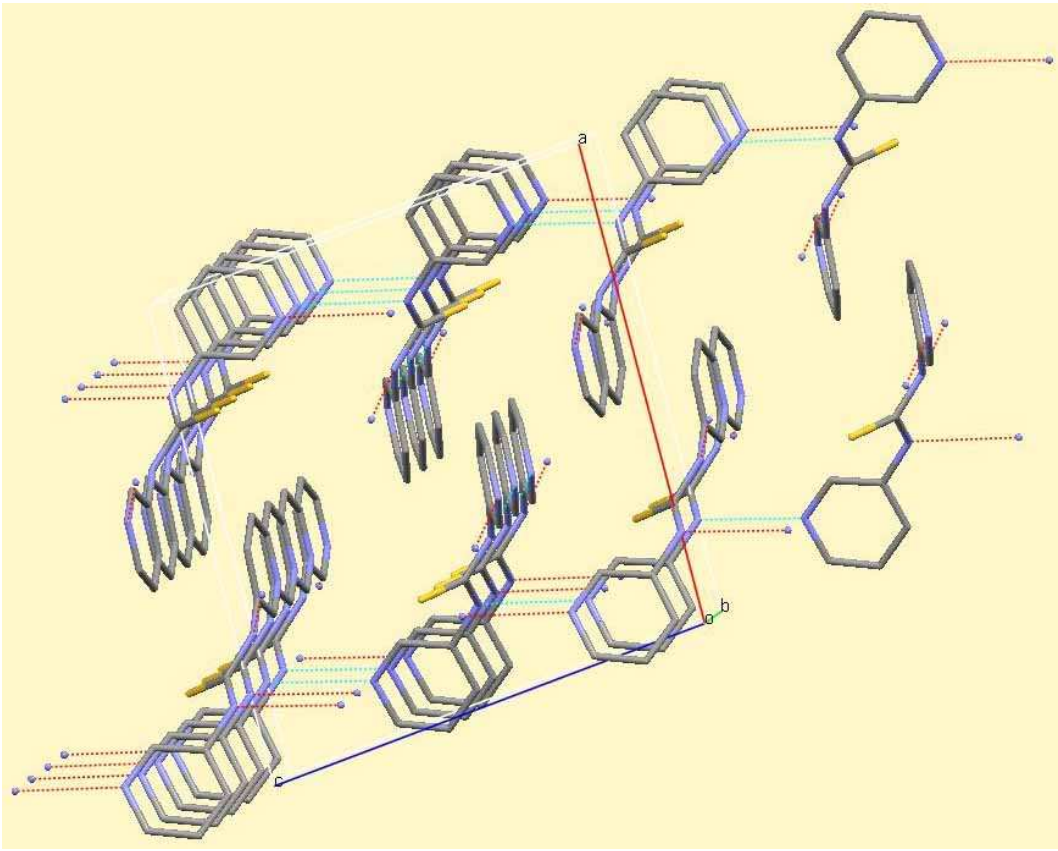

Figure 19: Hydrogen bonding network and packing diagram for **7**. Hydrogen atoms omitted for clarity

The 2D network structure of **7** results from two sets of Tu···Py interactions analogous to those that produce a 1D chain in **6**: N1–H···N3 and N2–H···N4. However, in the case of **7** both H-bonding interactions are geometrically forced to form intermolecularly and propagate in mutually perpendicular directions: parallel to the *b*- and *c*-axes. The sheets in **7** are not flat since the individual molecules are oriented at an angle of about 70° to the sheet plane. The sheets are comprised of bowl-shaped four-molecule H-bonded units which are tiled together.

A monohydrate of **6** (**6**•H_2O) has previously been reported [9]. It shows an EZ conformation. Interestingly, and in contrast to all of the diarylthioureas reported herein (see Table 4), both rings and the thiourea core in **6**•H_2O are virtually coplanar (<5° interplanar angles). The H-bonded structure of **6**•H_2O is analogous to that of **6**, consisting of both intra- and intermolecular H-bonding. However, the latter connects the thiourea nitrogen to the water of hydration, and a second intermolecular H-bond connects the water to a pyridyl ring. Thus, a zigzag chain results, in somewhat analogous fashion to **6**. Like structures **6** and **6**•H_2O, *N*,*N*′-bis(2-pyridyl)urea exists in the EZ conformation and has an internal H-bond [31]. However, in contrast to **6** and **6**•H_2O, it forms dimers via intermolecular N–H···O (urea···urea), instead of producing a chain. Like the thiourea **7**, *N*,*N*′-bis(3-pyridyl)urea adopts a ZZ conformation [27]. Although the interplanar angle between the two rings in the urea is only about 12.2° (versus 72.21(4)° for **7**), nevertheless, like the **7** molecules, the ureas form two sets of urea···Py H-bonds running in roughly perpendicular directions. These interactions result in formation of a sheet structure closely related to that of **7**. The urea molecules lie at an angle of about 45° to the overall H-bonded sheet.

3.1.1.4 (3-Py)TuMe **8**, *(2-Py)TuMe* **9**, *BztTuMe* **10**

Stoichiometry for these three thioureas was confirmed by elemental analysis, $^{1}H/^{13}C$ NMR, and IR data. Crystal growth for these thioureas was unsuccessful thus preventing the characterization of thiourea H-bonding networks. A CuI(BztTuMe) crystal was successfully isolated and the structure was solved. It proved identical to the known crystal structure (section 3.2.2.8).

3.2 Copper(I) Thiourea Complexes

The goal of the current project was to characterize various novel complexes of CuX (X = Cl, Br, I, or NO_3) with heterocyclic substituted thioureas (Tu). This work follows upon the synthesis of the novel Tu complexes previously discussed. It was hoped that the incorporation of nitrogen and sulfur centers into the Tu molecule would produce additional coordination sites for copper(I), resulting in oligomer formation.

Each CuX salt shows particular bonding trends that have been examined in detail and will be discussed in section 3.2.1. Because the majority of the CuX compounds used are soluble in MeCN, this solvent was used for most of the bulk reactions for consistency. However, some of the thioureas were insoluble in MeCN, necessitating the use of mixed solvent reactions. This solvent environment allowed for incorporation of not only with MeCN, but also acetone in some products. To prevent such undesirable interaction of reactants with additional solvent molecules, the use of acetone as solvent for thioureas that did not dissolve in MeCN was avoided in as many cases as possible. Instead, these thioureas were suspended in MeCN and slowly injected into the reaction flask thus promoting thorough mixing of both reactants.

In reactions involving $CuNO_3$ with 2-PyTuPh, 2-PyTuMe, 3-PyTuPh, 3-PyTuMe, PymTuMe, BztTuMe the molar ratio of Cu(I) to thiourea used was 1:2. In all of the other Cu(I) Tu coordination reactions, the reactants were introduced at a 1:1 molar ratio. In both cases, the resulting products showed surprising variability in their stoichiometry. Because the focus of this research was on characterizing the products, there was not adequate time to perform analogous reactions in different ratios. However, these preliminary findings indicate that there will probably be a wide range of complexes uncovered once various reactant ratios have been explored. Elemental analysis was the primary means of determining the product stoichiometry. All complexes were analyzed for the percent copper, and a few complexes were also analyzed for carbon, hydrogen, and nitrogen content. The elemental analysis data are conveyed in Table **5**.

However, simply knowing the stoichiometry is not enough to understand the structure of the complexes. Copper(I) prefers a four-coordinate environment. The use of heterocyclic Tu ligands allows construction of this coordination environment in an assortment of ways. Each Tu has, by its nature, two nitrogen and one sulfur atom, all of which provide potential coordination sites. Addition of each pyridyl ring provides an additional nitrogen site, and a pyrimidyl ring provides an additional two. Creation of four-coordinate copper with polydentate ligands is commonly accomplished by formation of a polymeric structure. To determine the nature of the metal coordination sphere, the selection of heteroatoms for coordination, the presence of hydrogen-bonding, and whether a particular complex is polymeric and what kind of geometry it maintained, X-ray crystallography was utilized whenever possible.

3.2.1 Product Stoichiometry and Elemental Analysis

In order to work with copper(I), one generally has to reduce copper(II) with a reducing agent. While the copper(I) halides are commercially available, copper(I) nitrate undergoes a spontaneous internal redox reaction. Therefore, $Cu(NO_3)$ had to be freshly generated *in situ*. This was accomplished through redox conproportionation, using copper(0), reaction (3):

$$Cu(NO_3)_2 + Cu \rightarrow 2\ Cu(NO_3) \qquad (3)$$

The reaction was determined to have gone to completion by observing the loss of the distinctive copper(II) color. Copper metal is added in excess, so it appears to remain unchanged throughout the reaction. Copper(II) compounds are blue, while copper(I) tend to be colorless or white depending on the phase. The $Cu(NO_3)_2$ was dissolved in acetonitrile, forming a blue solution. Upon completion of the reaction, the solution became colorless. The excess copper wire was removed, and the resulting solution was stable under a nitrogen environment. Copper(I) chloride and copper(I) bromide were purified by recrystallization in HCl and HBr and stored at temperatures below 0 ^{o}C; copper(I) iodide is stable at room temperature.

For the preparation of these thiourea complexes, all the CuX salts were dissolved in MeCN. In MeCN, copper(I) nitrate is colorless, copper(I) bromide is a pale green solution, copper(I) iodide is a pale yellow solution, and copper(I) chloride is a dark yellow solution. Upon addition of the thiourea, in almost every case, there was a color change and an immediate precipitation. To ensure that the reaction went to completion, the reactions were allowed to stir under nitrogen for an hour. In all syntheses except one, the thiourea was added to the copper-containing solution as a solid. The exception

occurred in the synthesis of $CuNO_3$(3-PyTuPh)•acetone because earlier crystal structures had indicated that the complex incorporated acetone. Elemental analysis was the first analytical technique employed to verify the identity of the new complexes. The results are summarized in Table **5**. Unless otherwise indicated, the percent values refer to copper.

Table **5**: Elemental Analysis for Novel Copper Complexes (Bulk reaction)

Complex	Yield %	Color	Analysis (Theory) %
$CuCl(2\text{-}PyTuPh)_2$	68.5	White	Cu 9.8 (11.4)
			C 52.08 (51.70)
			H 3.97 (3.98)
			N 15.13 (15.70)
$(CuCl)_2(2\text{-}PyTuMe)_3$	75.1	White	Cu 18.9 (18.2)
			C 35.88 (36.05)
			H 3.81 (3.89)
			N 17.81 (18.02)
$CuCl(3\text{-}PyTuPh)_3$	81.3	Yellow	Cu 8.6 (8.0)
CuCl(3-PyTuMe)	72.9	White	Cu 23.0 (23.9)
(CuCl)(4-PyTuPh)	74.0	Yellow	Cu 17.7 (19.4)
			C 43.69 (43.90)
			H 3.32 (3.38)
			N 12.88 (12.80)
$CuCl(PymTuPh)_2$	85.1	White	Cu 11.7 (11.4)
			C 47.19 (47.22)

			H 3.66 (3.60)
			N 19.76 (20.02)
$CuCl(PymTuMe)_4$	85.0	Brown	Cu 15.1 (8.2)
			C 37.84 (37.35)
			H 4.27 (4.18)
			N 29.22 (29.03)
CuCl(BztTuMe)•0.5MeCN	87.6	Yellow-white	Cu 18.3 (18.5)
			C 35.20 (35.03)
			H 3.03 (3.09)
			N 13.85 (14.30)
$(CuCl)_2(ThzTuMe)_3$	57.3	White	Cu 18.2 (17.7)
			C 25.24 (25.10)
			H 2.93 (2.95)
			N 17.50 (17.71)
$(CuCl)_2[(2\text{-}Py)_2Tu]_3$	68.7	Yellow	Cu 15.2 (14.3)
			C 43.54 (44.59)
			H 3.36 (3.40)
			N 18.63 (18.91)
$CuCl[(3\text{-}Py)_2Tu]_4$	81.9	Pale Green	Cu 5.9 (6.2)
			C 52.09 (51.80)
			H 3.97 (3.95)
			N 21.79 (21.97)
CuBr(2-PyTuPh)•MeCN	77.6	Grey-green	Cu 14.6 (15.4)

			C 42.44 (40.64)
			H 3.42 (3.41)
			N 13.53 (13.54)
CuBr(2-PyTuMe)•0.5MeCN	62.8	Cream	Cu 18.9 (18.1)
			C 31.41 (30.73)
			H 3.43 (3.44)
			N 15.62 (15.93)
$(CuBr)_2(3\text{-PyTuPh})_3$•acetone	91.9	Light brown	Cu 13.8 (13.0)
CuBr(3-PyTuMe)•MeCN	62.9	Cream	Cu 18.1 (18.1)
CuBr(4-PyTuPh)	48.4	Yellow	Cu 16.7 (17.0)
			C 39.07 (38.67)
			H 3.04 (2.97)
			N 11.62 (11.27)
CuBr(PymTuPh)	85.4	Cream-yellow	Cu 19.0 (19.3)
CuBr(PymTuMe)	78.5	Cream-yellow	Cu 21.1 (20.4)
			C 23.47 (23.12)
			H 2.59 (2.59)
			N 17.99 (17.98)
CuBr(BztTuMe)	72.0	Yellow-green	Cu 16.3 (17.3)
			C 29.17 (29.47)
			H 2.57 (2.47)
			N 11.31 (11.46)
$(CuBr)_2(ThzTuMe)_3$	80.5	White	Cu 16.0 (15.8)

			C 22.53 (22.33) H 2.63 (2.62) N 15.66 (15.63)
$CuBr[(2\text{-}Py)_2Tu]$	79.7	Yellow	Cu 19.8 (16.9) C 35.11 (35.35) H 2.74 (2.70) N 15.08 (14.99)
$CuBr[(3\text{-}Py)_2Tu]_5$		Grayish white	Cu 4.8 (4.9) C 51.71 (51.02) H 3.98 (3.89) N 21.62 (21.63)
CuI(2-PyTuPh)	94.5	White	Cu 15.0 (15.1) C 34.24 (34.34) H 2.63 (2.64) N 10.05 (10.01)
CuI(2-PyTuMe)•MeCN	88.2	Cream	Cu 16.1 (15.9) C 27.88 (27.11) H 3.01 (3.03) N 13.86 (14.05)
CuI(3-PyTuPh)	86.2	Pale yellow	Cu 15.3 (15.1) C 33.62 (34.34) H 2.66 (2.64) N 10.22 (10.01)

CuI(3-PyTuMe)	94.1	White	Cu 18.3 (17.8)
			C 23.57 (23.51)
			H 2.57 (2.54)
			N 11.56 (11.75)
CuI(4-PyTuPh)	82.3	Yellow	Cu 17.6 (15.5)
			C 34.89 (34.34)
			H 2.66 (2.64)
			N 9.91 (10.01)
(CuI)(PymTuPh)	54.2	Yellow	Cu 20.7 (15.10)
			C 30.67 (31.40)
			H 2.35 (2.40)
			N 13.07 (13.32)
$(CuI)_2(PymTuMe)_2$	97.5	Pale yellow	Cu 21.1 (20.4)
$(CuI)_2(BztTuMe)_3$	88.8	Yellow	Cu 14.2 (12.1)
			C 30.04 (30.86)
			H 2.58 (2.59)
			N 11.88 (12.00)
CuI(ThzTuMe)	68.6	Yellow	Cu 18.2 (19.0)
			C 16.90 (16.51)
			H 1.93 (1.94)
			N 11.58 (11.55)
CuI[$(2\text{-Py})_2$Tu]	79.0	Cream	Cu 15.5 (15.0)
			C 31.50 (31.40)

			H 2.46 (2.40)
			N 13.47 (13.32)
$CuI[(3\text{-}Py)_2Tu]_4$	82.9	Pale yellow	Cu 5.5 (5.7)
			C 48.44 (47.54)
			H 3.78 (3.63)
			N 20.48 (20.16)
$(CuNO_3)_2(2\text{-}PyTuPh)_3$	≈95	Light brown	Cu 12.6 (13.3)
			C 44.28 (46.05)
			H 3.38 (3.54)
			N 15.81 (16.41)
$(CuNO_3)(2\text{-}PyTuMe)$•MeCN	89.2	White	Cu 19.2 (19.0)
			C 31.97 (32.38)
			H 3.51 (3.62)
			N 20.65 (20.98)
$CuNO_3(3\text{-}PyTuPh)$•MeCN	90.4	Yellow	Cu 15.6 (16.1)
			C 42.84 (42.47)
			H 3.64 (3.56)
			N 17.43 (17.69)
$CuNO_3(3\text{-}PyTuMe)$•2MeCN	80.2	Off white	Cu 18.4 (17.0)
$(CuNO_3)_2(4\text{-}PyTuPh)_3$	41.8	White	Cu 15.3 (13.5)
			C 45.02 (46.05)
			H 3.48 (3.54)
			N 15.64 (16.41)

$CuNO_3$(PymTuPh)	53.1	Yellow	Cu 11.8 (10.8) C 45.14 (45.08) H 3.44 (3.44) N 21.51 (21.51)
$(CuNO_3)_2$(PymTuMe)$_3$	71.4	Yellow	Cu 16.6 (16.8)
$CuNO_3$(BztTuMe)•MeCN	63.4	Light green	Cu 19.0 (16.3) C 34.32 (33.88) H 3.07 (3.10) N 17.38 (17.96)
$(CuNO_3)$(ThzTuMe)$_2$	7.4	Light brown	Cu 14.8 (13.5) C 25.41 (25.44) H 2.80 (2.99) N 20.16 (20.77)
$(CuNO_3)_2[(2Py)_2Tu]_3$•MeCN 1 hour time scale	24.8	Yellow	Cu 11.8 (12.93) C 43.11 (42.76) H 3.44 (3.38) N 20.91 (21.37)
$CuNO_3[(2Py)_2Tu]_2$ 4 hour time scale	45.0	Orange	Cu 11.3 (10.8) C 45.05 (45.08) H 3.41 (3.44) N 21.50 (21.51)
$CuNO_3[(3\text{-}Py)_2Tu]$•MeCN	80.4	Yellow	Cu 15.7 (16.0) C 39.77 (39.34)

	H 3.36 (3.30)
	N 20.94 (21.17)

Based on these data, the stoichiometry of each complex was determined. Table **6** summarizes the stoichiometries of the copper halide thiourea complexes prepared in this project. The product ratios are expressed as CuX:thiourea, e.g. 1:2 CuCl:PymTuMe = $CuCl(PymTuMe)_2$. For simplicity, all ratios are represented as whole numbers.

Table **6a**: Copper(I) Salt Heterosubstituted Thiourea Complex Metal:Ligand Ratios

	CuCl	CuBr	CuI	$CuNO_3$
2-PyTuPh	1:2	1:1•MeCN	1:1	2:3
2-PyTuMe	2:3	1:1•0.5MeCN	1:1•MeCN	3:2
3-PyTuPh	1:3	2:3•acetone	1:1	1:1•MeCN
3-PyTuMe	1:1	1:1•MeCN	1:1	1:1•2MeCN
4-PyTuPh	1:1	1:1	1:1	2:3
PymTuPh	1:2	1:1	1:1	1:1
PymTuMe	1:4	1:1	2:2	2:3
BztTuMe	1:1•0.5MeCN	1:1	2:3	1:1•MeCN
ThzTuMe	2:3	2:3	1:1	1:2
$(2Py)_2Tu$	2:3	1:1	1:1	2:3•MeCN (1 hr) 1:2 (4 hr)
$(3Py)_2Tu$	1:4	1:5	1:4	1:1•MeCN

Examining the molar ratios in Table **6a** allows for a discernment of a few trends with regard to both particular ligands and copper halides. The most notable trend among the copper halides is the preference of 1:1 metal to ligand ratios for copper(I) bromide and copper(I) iodide complexes. In the case of copper(I) bromide complexes, the only exception to this trend occurs with 3PyTuPh, ThzTuMe, and $(3Py)_2Tu$. In the case of copper(I) iodide, the only exception to this trend occurs with PymTuMe, BztTuMe, and $(3Py)_2Tu$. The remaining two copper salts, chloride and nitrate, do not seem to follow a strict set of guidelines, but instead reveal varying product ratios, from 1:1 to 1:5 copper salt:thiourea.

There are also a few trends associated with each thiourea that are noteworthy. Some trends, such as the fact that 3-PyTuMe only forms products in a 1:1 ratio, are readily discernable. The next thing to note is the incorporation of solvent molecules in the complexes. Copper(I) chloride and copper(I) iodide show very rare cases (only one each) of solvent molecule incorporation. Copper(I) bromide complexes show solvent molecule incorporation in the upper half of the table with ligands containing 2-pyridyl and phenyl/methyl substituents on the thiourea. Copper(I) nitrate complexes on the hand primarily incorporate solvent molecules in the lower half of the table with ligands that have more than three nitrogen atoms or more than one sulfur atom. Solvent incorporation is also seen for copper(I) nitrate complexes with thioureas containing a 3-pyridyl ring.

The reaction of copper(I) nitrate with $(2\text{-}Py)_2Tu$ showed varied results with a change in reaction time. When the reaction was allowed to run for one hour, a yellow precipitate formed. Elemental analysis suggested that this product was $(CuNO_3)_2[(2Py)_2Tu]_3 \bullet MeCN$. When the time scale was lengthened to four hours, an

orange precipitate formed. Elemental analysis results suggested this complex to be $CuNO_3[(2Py)_2Tu]_2$. When crystals for X-ray were grown, distinct yellow and orange crystals were isolated within a single tube. An orange crystal proved to have the composition $CuNO_3[(2Py)_2Tu]_2$, as also predicted by elemental analysis. A yellow crystal solved as $(CuNO_3)_2(patp)_2$•MeCN having a cyclized dipyridyltetraazathiapentalene (patp) ligand. Patp was first synthesized by Rong-Bin Huang in which the oxidation of 2-aminopyridine in carbon disulfide was carried out in open air [29]. We propose that $CuNO_3$ initially reacts with $(2Py)_2Tu$ to form a stable intermediate, $(CuNO_3)_2[(2Py)_2Tu]_3$•MeCN. This is the yellow precipitate isolated after one hour in the bulk reaction. Upon extending the reaction time scale the intermediate complex converts to the orange colored and relatively stable $CuNO_3[(2Py)_2Tu]_2$. This suggestion is supported by elemental analysis and the X-ray structure obtained. When the reaction time is extended beyond four hours (as is the case with slow crystallization), the nitrogen atoms found on each ring on the thiourea align favorably to cyclize the ligand, forming $(CuNO_3)_2(patp)_2$•MeCN. This proposed cyclization mechansim is described in Scheme 1. The structures of $CuNO_3[(2Py)_2Tu]_2$ and $(CuNO_3)_2(patp)_2$•MeCN and discussed in section 3.2.2.10.

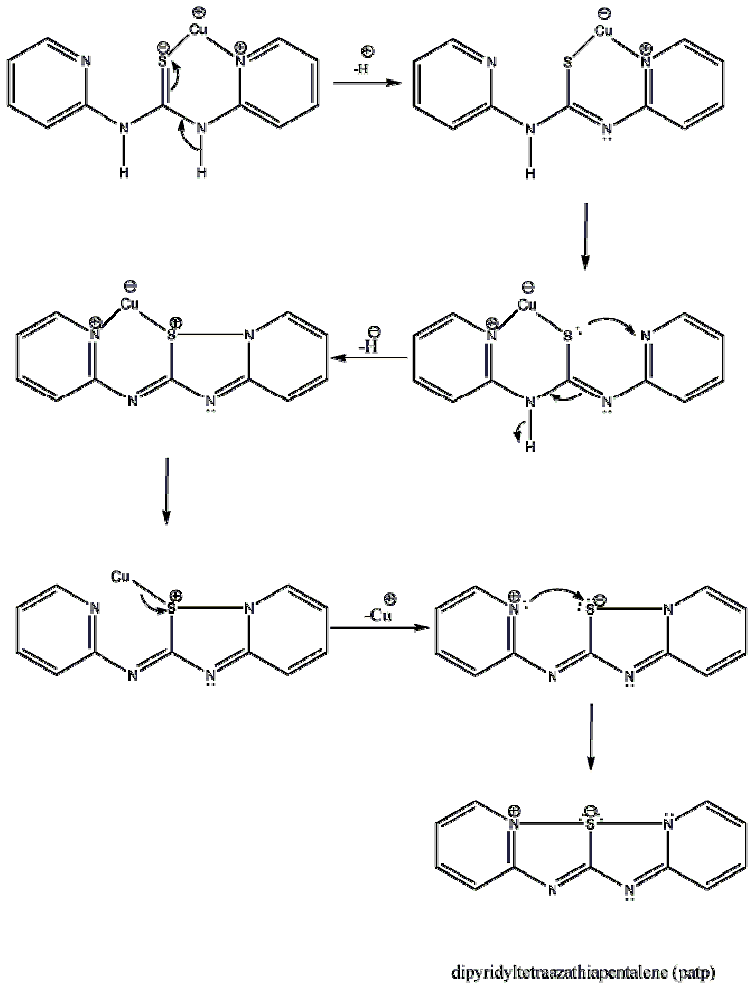

Scheme 1: Proposed mechanism for formation of patp

When each ligand is considered separately, the metal:ligand ratios seem to have one dominant ratio, usually with one exception or two at most. For example, the 4-PyTuPh shows a metal:ligand ratio preference of 1:1 with an exception of the complex with copper(I) nitrate which shows a ratio of 2:3. Such trends suggest that complexes coordinating the same thiourea might have similar structures, despite the difference in halide and nitrate.

Initially, the reaction between copper(I) bromide and 3-PyTuPh took place in MeCN. With this solvent, 3-PyTuPh seemed to remain unreacted or to react to an unidentifiable product. However, upon changing to acetone, the reaction proceeded

smoothly. This is noteworthy because, even though 3-PyTuPh is not the only thiourea that was insoluble in MeCN, it was the only Tu which was unable to complete the reaction when introduced as a solid and vigorously stirred with copper(I) bromide. The incorporation of solvent molecules is better understood with the help of X-ray analysis, but this technique was only viable with some of the complexes.

Table **5** and **6a** show proposed metal:ligand ratios based on Cu and C/H/N analysis (elemental analysis). It is not uncommon to find single crystals grown for X-ray crystallography purposes to have a different structure than their bulk syntheses counterpart. Table **6b** shows the confirmed structures of a few complexes whose crystal were successfully grown and analyzed by X-ray crystallography and whose X-ray confirmed metal:ligand ratios did not match the metal:ligand ratios proposed by elemental analysis. The ratios as proposed by elemental analysis are also repeated alongside so as to make comparison easier.

Table **6b**: Copper(I) Complexes Metal:Ligand ratios (X-ray analysis)

CuX + Tu	Metal:Ligand (X-ray analysis)	Metal:Ligand (Elemental analysis)
CuCl + PymTuMe	1:2	1:4
CuCl + $(2\text{-Py})_2$Tu	2:2	2:3
CuBr + 2-PyTuPh	1:2	1:1•MeCN
CuBr + 3-PyTuPh	2:3	2:3•acetone
CuBr + BztTuMe	1:2	1:1
CuI + BztTuMe	1:1	2:3
$CuNO_3$ + 3-PyTuPh	1:1	1:1•MeCN

One important trend that is made obvious from table **6b** is the fact that none of the X-ray complexes show incorporation of a solvent molecule. Also, out of the eleven copper complexes discussed in this paper, table **6b** shows seven complexes where the metal:ligand ratios from X-ray analysis and from elemental analysis do not match. There may be several reasons for this discrepancy. While growing crystals, the solvent used to dissolve copper was acetonitrile and acetone for the thiourea. As for bulk reactions, the solvent for both the metal and the thiourea was acetonitrile. This change is environment could have affected the results seen in table **6b**. It is also possible that since bulk reactions were run for a short time scale, while crystals were allowed to grow for a far longer time, the former could be the kinetic product while the latter could be the thermodynamic product.

3.2.2 X-ray crystallography

Crystal growth techniques for thioureas have been discussed previously in Section 2.3.2. X-ray quality crystals were produced for seven thioureas. Table **7** and Table **8** below show selected bond distances (Å) and angles (˚) respectively.

Table 7: Bond lengths for Cu(I) complexes (atom assignment shown when necessary):

Complex	Cu-Cu (Å)	Cu-X (Å)	Cu-S (Å)	Cu-N (Å)
$CuCl(PymTuPh)_2$	-	2.2497(5)	2.2141(5)	-
$CuCl(PymTuMe)_2$	-	2.2557(5)	2.2189(5)	-
$(CuCl)_2[(2\text{-}Py)_2Tu]_2$	3.0049(5)	2.4070(4)	2.2475(4)	2.0642(13)
$CuBr(2\text{-}PyTuPh)_2$	3.897	2.4395(3)	2.2611(6) Cu1a-S1 2.5169(6) Cu1a-S2a	-
$(CuBr)_2(3\text{-}PyTuPh)_3$	-	2.487	2.303 Cu1-S 2.271 Cu2-S	2.095 Cu1-N 2.079 Cu2-N
$CuBr(BztTuMe)_2$	-	2.4216(4)	2.2355(7)	-
$(CuI)_2(PymTuMe)_2$	2.7927(9) Cu1-Cu2	2.6064(6) Cu1-I1 2.6587(7) Cu1-I2	2.3426(12) Cu1-S1 2.4203(12) Cu1-S2	-
CuI(BztTuMe)	2.7194(17) Cu_2I_2 rhomboid 3.0171(17) Cu_2S_2 rhomboid	2.6553(7)	2.3185(15) Cu-S	-
$[Cu(3\text{-}PyTuPh)_2]NO_3$	-	-	2.3100(4) Cu1-S1 2.2792(4) Cu1-S2	2.0629(13)
$[Cu\{(2\text{-}Py)_2Tu\}_2]NO_3$	-	-	2.2846(5) Cu1-S1 2.2178(5) Cu1-S2	2.0954(15) Cu1-N2 2.0069(15) Cu1-N6
$(CuNO_3)_2(patp)_2{\cdot}MeCN$	2.672	-	-	1.971 Cu2-N6 2.103 Cu2-N11 1.916 Cu1-N1

Table **8**: Bond angles for Cu(I) complexes(atom assignments shown when necessary):

Complex	Angle	Bond angle (˚)
$CuCl(PymTuPh)_2$	S1-Cu1-S2	117.671(18)
	S1-Cu1-Cl1	120.021(18)
	S2-Cu1-Cl1	122.308(18)
$CuCl(PymTuMe)_2$	S2-Cu1-S1	119.64(2)
	S1-Cu1-Cl1	120.60(2)
$(CuCl)_2[(2\text{-}Py)_2Tu]_2$	N4-Cu1-S1	118.24(4)
	N4-Cu1-Cl1	109.02(4)
	N4-Cu1-Cl2	100.85(4)
	S1-Cu1-Cl1	108.578(16)
	S1-Cu1-Cl1	115.840(16)
	Cl2-Cu1-Cl1	103.099(14)
	Cu1-Cl1-Cu2	76.900(14)
$CuBr(2\text{-}PyTuPh)_2$	S2-Cu1-Br1	114.951(18)
	S1-Cu1-Br1	123.079(18)
	S2-Cu1-S1	105.79(2)
$(CuBr)_2(3\text{-}PyTuPh)_3$	S-Cu1-S	105.71(9)
	S-Cu1-N	111.0(2)
	Br-Cu1-N	104.47(19)
	Br-Cu1-S	117.96(7)
	S-Cu2-N	108.57(19)
	N-Cu2-N	98.1(3)
	N-Cu2-Br	106.7(2)
	S-Cu2-Br	120.98(7)
$CuBr(BztTuMe)_2$	S-Cu-S	114.72(3)
	S-Cu-Br	122.41(2)
$(CuI)_2(PymTuMe)_2$	Cu1-I1-Cu2	64.057(19)
	S1-Cu2-S2	102.79(4)
	S2-Cu1-I2	118.47(4)
	S1-Cu2-I1	109.50(3)
	S1-Cu1-I2	102.88(3)
	S2-Cu1-I2	108.67(3)
	I1-Cu1-I2	113.65(2)
	S1-Cu1-Cu2	144.26(4)
	S2-Cu1-Cu2	111.55(4)
	I1-Cu1-Cu2	58.881(18)
CuI(BztTuMe)	S-Cu-S	101.06(5)
	I-Cu-I	117.87(3)
$[Cu(3\text{-}PyTuPh)_2]NO_3$	N6-Cu1-N3	101.02(5)
	N6-Cu1-S2	118.90(4)
	N3-Cu1-S2	111.48(4)
	N6-Cu1-S1	101.16(4)
	N3-Cu1-S1	106.99(4)
	S2-Cu1-S1	115.614(16)

$[Cu\{(2\text{-}Py)_2Tu\}_2]NO_3$	N6-Cu1-N2 N6-Cu1-S2 N2-Cu1-S2 N6-Cu1-S1 N2-Cu1-S1 S2-Cu1-S1	109.15(6) 101.16(4) 108.53(4) 115.55(4) 91.67(4) 129.354(19)
$(CuNO_3)_2(patp)_2$•MeCN	N2-Cu2-N6 N11-Cu2-N6	152.29 106.01

Bond lengths and bond angles most relevant for particular complexes are selected and discussed below.

3.2.2.1 $CuCl(PymTuPh)_2$

Crystals of $CuCl(PymTuPh)_2$ could not be grown in pure acetonitrile. A crystal growth tube was roughly half filled with 20mM CuCl and layered with 20mM PymTuPh in acetone. The structure obtained is shown in Figure 20.

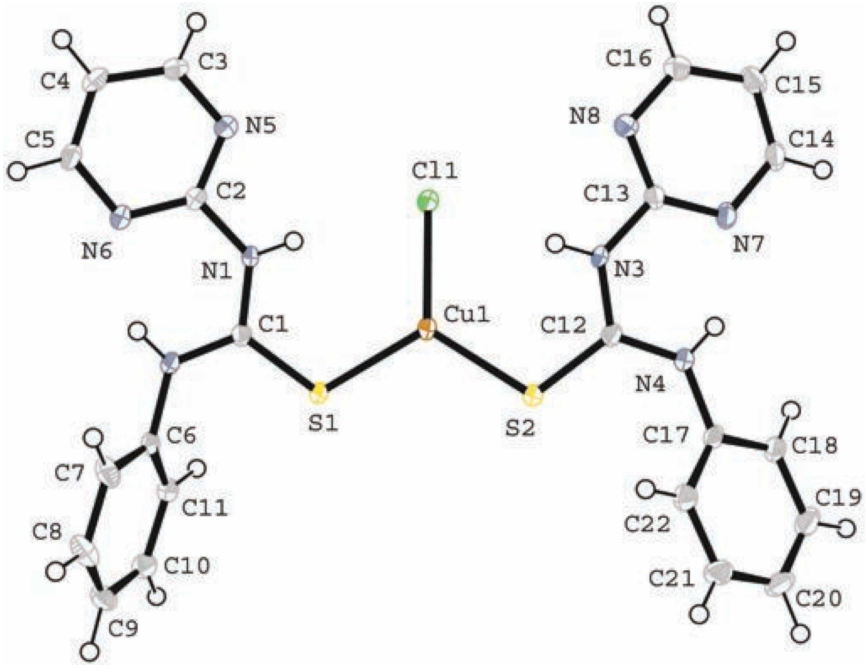

Figure 20: $CuCl(PymTuPh)_2$ molecular diagram

Interestingly, this complex is neither tetrahedral nor even four-coordinate, but instead adopts a trigonal planar geometry. Each copper coordinates directly to two sulfurs from

the two thioureas. The Cu–Cl bond length is 2.2497Å while the Cu–S bonds are around 2.2141 Å. The bond angles around the central copper atom are 117.67˚, 120.02, and 122.31˚, nearly perfect trigonal planar angles. The structure did not show any other interesting interactions.

3.2.2.2 $CuCl(PymTuMe)_2$

Crystals of $CuCl(PymTuMe)_2$ could not be grown in pure acetonitrile. A crystal growth tube was roughly half filled with 20 mM CuCl and layered with 20 mM PymTuMe in acetone. The structure obtained is shown in Figure 21.

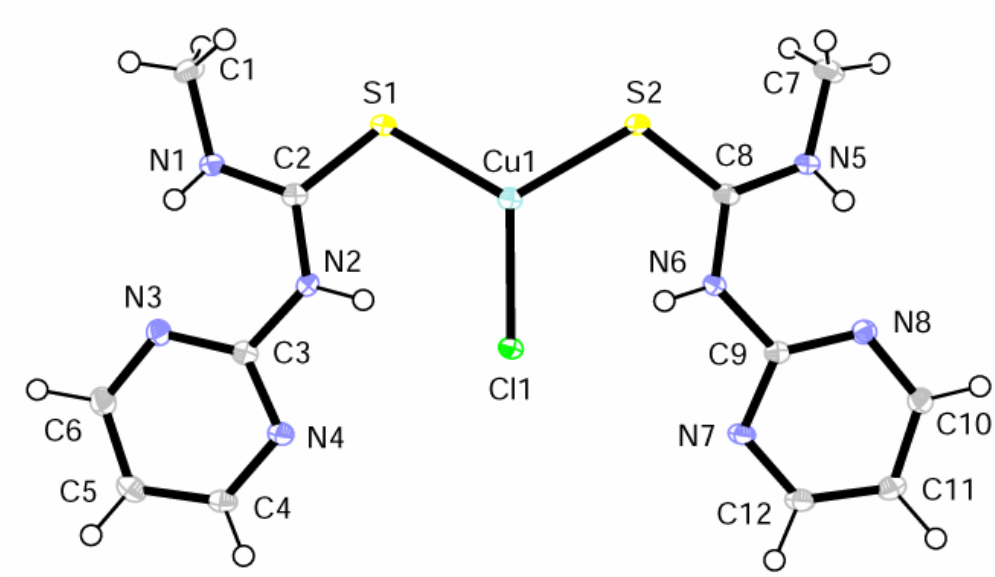

Figure 21: $CuCl(PymTuMe)_2$ molecular diagram

The $CuCl(PymTuMe)_2$ complex shares a lot of similarities with $CuCl(PymTuPh)_2$. Again, the copper is three-coordinate, bound to two sulfur atoms and one chlorine atom, and adopts a trigonal planar geometry. The Cu-Cl bond length is 2.2557 Å while the Cu–S bonds are around 2.2189 Å. The bond angles around the central copper atom are 120.60˚ and 119.63˚, nearly perfect trigonal planar angles. The structure did not show any other interesting interactions.

3.2.2.3 $(CuCl)_2[(2\text{-}Py)_2Tu]_2$

Crystals of $(CuCl)_2[(2\text{-}Py)_2Tu]_2$ could not be grown in pure acetonitrile. A crystal growth tube was roughly half filled with 20 mM CuCl and layered with 20 mM $(2\text{-}Py)_2Tu$ in acetone. The structure obtained is shown in Figure 22.

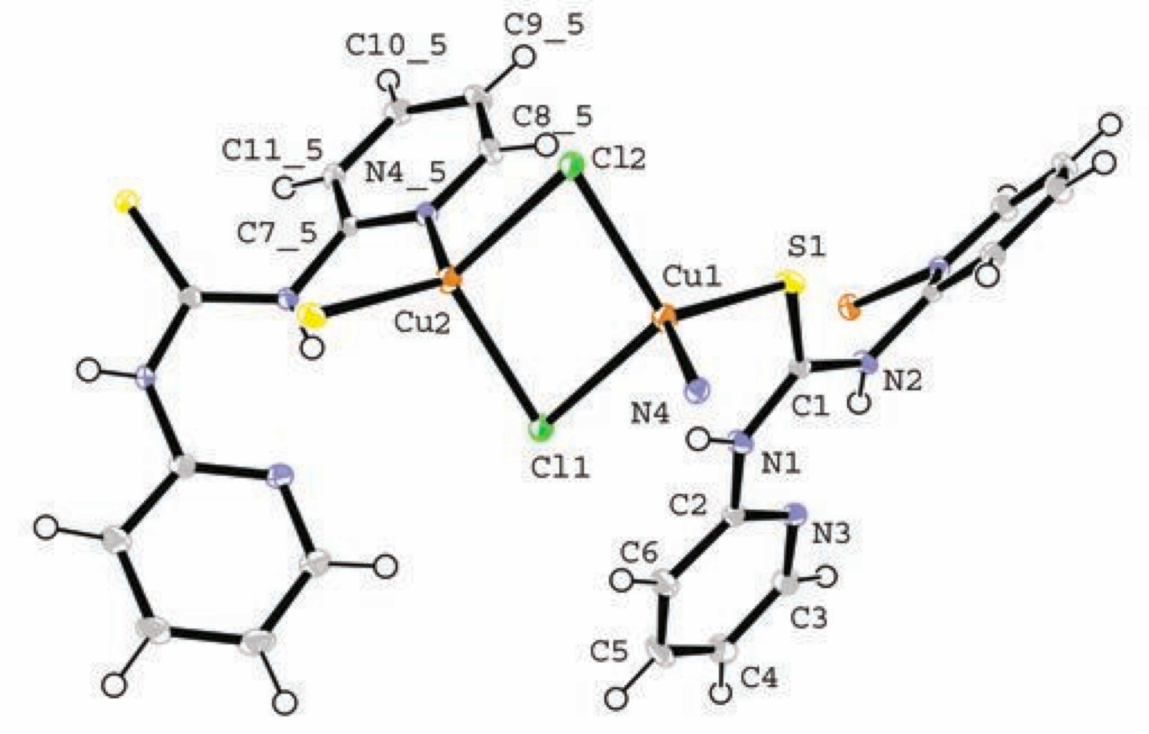

Figure 22: $(CuCl)_2[(2\text{-}Py)_2Tu]_2$ molecular diagram.

Unlike the previously discussed structures, the $(CuCl)_2[(2\text{-}Py)_2Tu]_2$ complex contains two four-coordinate copper atoms that are bridged by two chlorine atoms. The two copper atoms independently interact with a nitrogen and a sulfur atom made available from the thioureas. Thus the copper atoms adopt a roughly tetrahedral geometry. The N–Cu–S bond angle was found to be approximately 118.24˚, and the N–Cu–Cl bond angle approximated to 109.02˚. The rhomboid structure linking the two thioureas together comprising of two copper and two chlorine atoms had a Cu–Cl–Cu bond angle of 76.90˚, and a Cl–Cu–Cl bond angle of 103.01. The various bond lengths were found to be: Cu–

Cu 3.0049 Å, Cu–Cl 2.4070 Å, Cu–S 2.2475 Å, and Cu–N 2.0642 Å. Thus, there is almost no Cu–Cu interaction in this complex. The complex showed H-bonding interaction thus extending its network as seen in Figure 23.

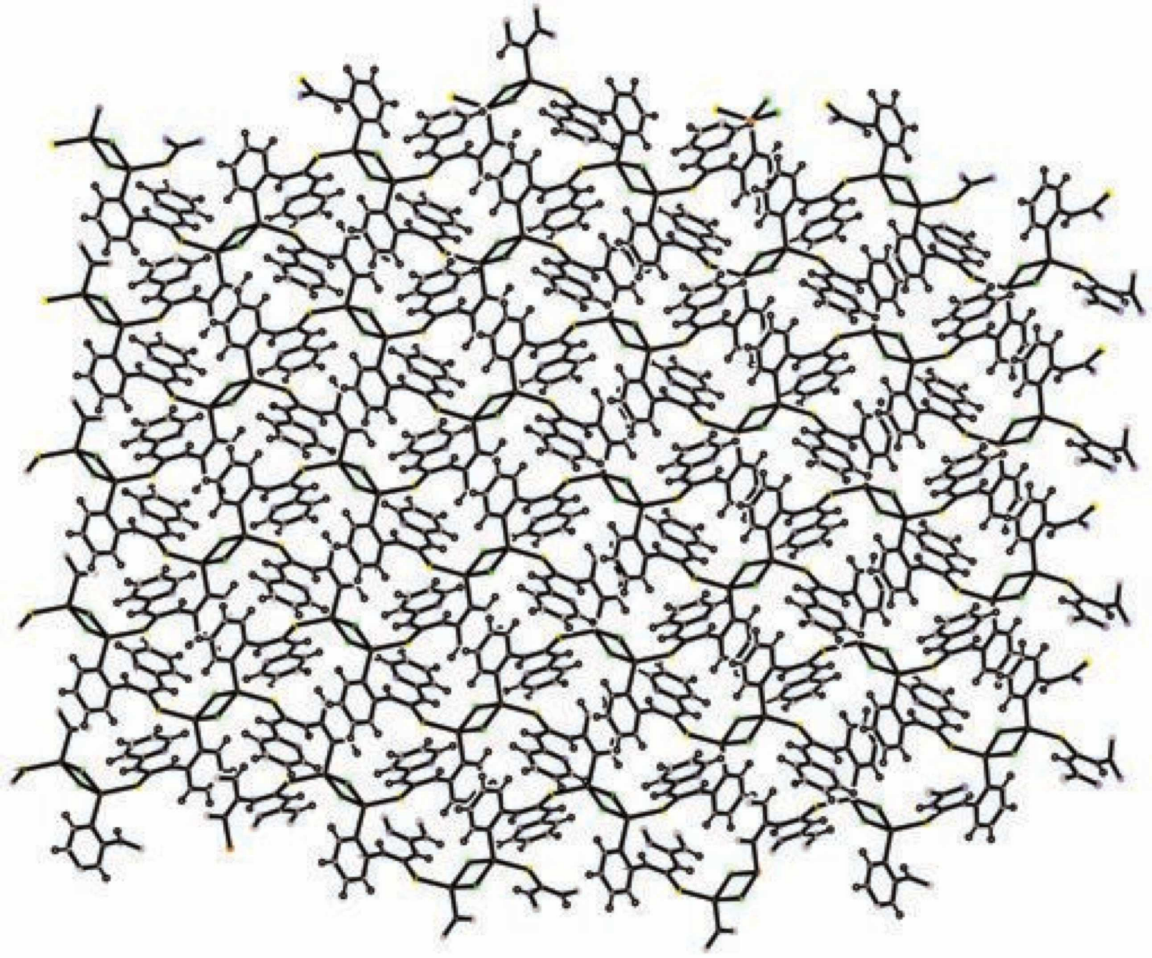

Figure 23: $(CuCl)_2[(2\text{-}Py)_2Tu]_2$ network interaction.

The $(CuCl)_2[(2\text{-}Py)_2Tu]_2$ network extends only along two axes thus giving it a two-dimensional sheet structure. It is capped off in the third axis by the non-coordinating thiourea rings. Holes and vacancies seen within the network could suggest its potential use as a trapping agent for small molecules.

3.2.2.4 $CuBr(2\text{-}PyTuPh)_2$

Crystals of $CuBr(2\text{-}PyTuPh)_2$ were grown from 20 mM CuBr in acetonitrile layered with 20 mM (2-PyTuPh) in acetone. The structure obtained is shown in Figure 24.

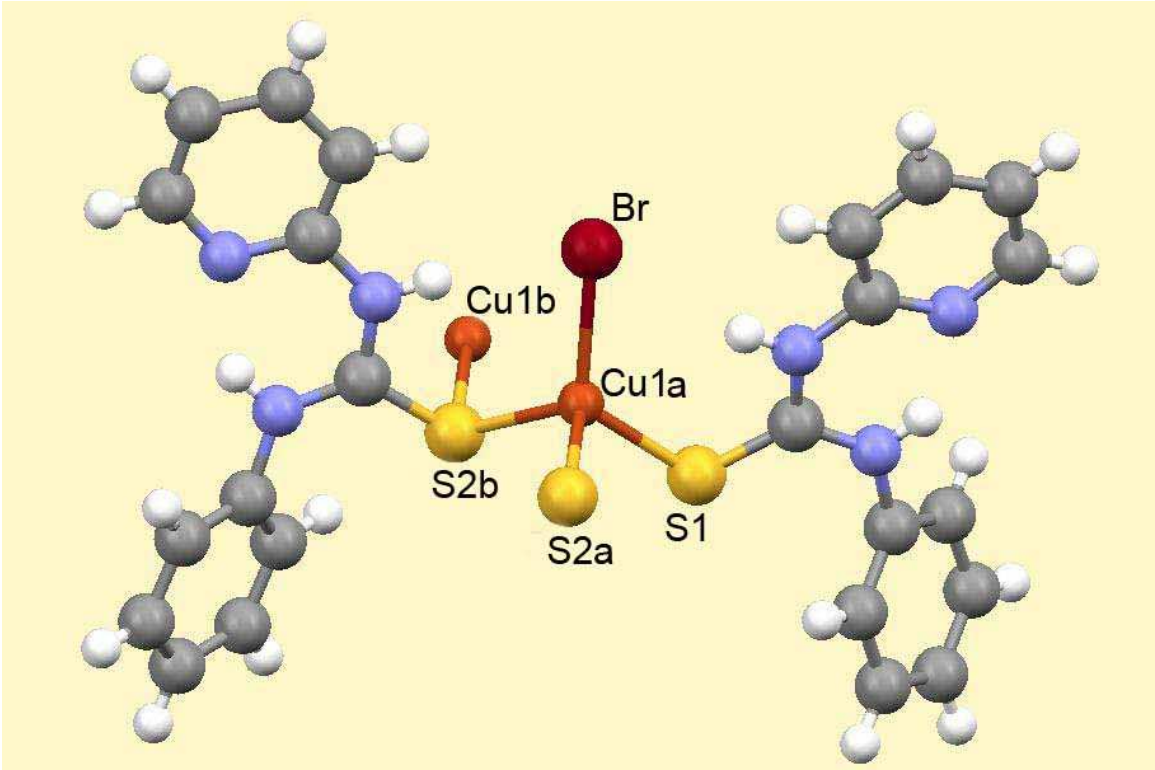

Figure 24: $CuBr(2\text{-}PyTuPh)_2$ molecular diagram

Though the unit cell consists of one CuBr molecule and two 2-PyTuPh thioureas, Figure 24 is provided to show two additional bonds, one involving the central copper atom and a sulfur atom coming out of the plane of the paper, while the second bond involves another sulfur atom bonding with the copper atom going into the plane of the paper. These bonds are shown to emphasize the central copper atoms four-coordinate tetrahedral geometry. Selected bond lengths around the copper atom were found to be: S2b–Cu1a–Br 114.95˚, S1–Cu1a–Br 123.08˚, S1–Cu1a–Br 103.58˚, Cu1a–S2b–Cu1b 107.44˚. The $CuBr(2\text{-}PyTuPh)_2$ complex is by far the most interesting structure found. Though the copper and sulfur atoms

are labeled differently, this is done solely to point out the various bond angles more simply. In actuality, Cu1a and Cu1b atoms are symmetrically identical. In the case of sulfur atoms, not only are the S2a and S2b atoms symmetrically identical, they are in fact the same atom. The structural arrangement is better explained with the help of Figure 25.

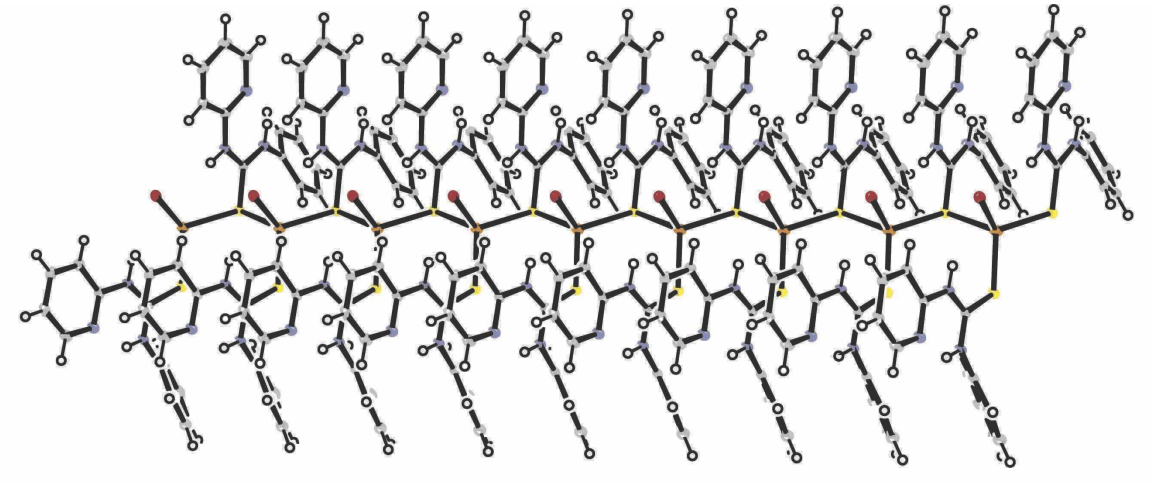

Figure 25: $CuBr(2\text{-}PyTuPh)_2$ polymer structure.

As can be seen from the above structure, apart from coordinating to bromide, copper also coordinates with two thiourea molecules on either side. Interestingly, one sulfur atom is bridging while the other is monodentate. This unusual distinction between the two thioureas leads to distortion of bond angles. The complex forms a one-dimensional linear chain capped on either sides by thiourea molecules. The bond lengths were found to be: Cu1a–S2a 2.517 Å, Cu1a–S1 2.261 Å, Cu1–Br 2.439 Å, and Cu1a–Cu1b 3.897 Å. The Cu–Cu distance is too long for any sort of interaction between the two atoms.

3.2.2.5 $(CuBr)_2(3\text{-}PyTuPh)_3$

Crystals of $(CuBr)_2(3\text{-}PyTuPh)_3$ were grown from 20 mM CuBr in acetonitrile layered with 20 mM (3-PyTuPh) in acetone. Unfortunately, only a low quality X-ray

structure could be obtained, however, the resulting structure is fairly complex, and is shown in Figures 26 and 27.

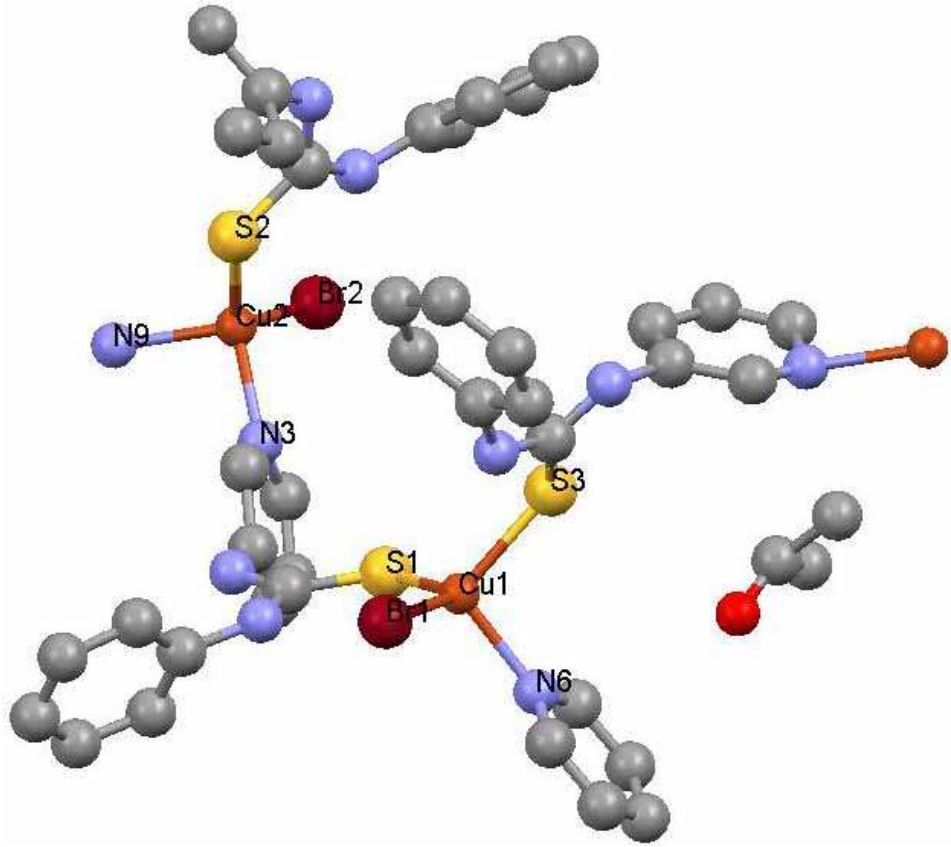

Figure 26: $(CuBr)_2(3\text{-}PyTuPh)_3$ molecular diagram. Hydrogen atoms omitted for clarity.

The structure has two distinct copper atoms. One of them coordinates to a bromide atom, a nitrogen atom from one thiourea ring, and two sulfur atoms from two more thioureas. The second copper atom coordinates with a bromide atom, a sulfur atom from one thiourea molecule, and two nitrogen atoms from two more thioureas. Selected bond lengths around the copper atom were found to be: Cu–Br 2.487 Å, Cu1–S 2.303 Å, Cu1–N6 2.095 Å, Cu2–S2 2.271 Å, Cu2–N 2.079 Å. Selected bond angles around copper were found to be: S–Cu1–S 105.71˚, S–Cu1–N 110.95˚, Br–Cu1–N 104.47˚, Br–Cu1–S 117.96˚, S–Cu2–N 108.59˚, N–Cu2–N 98.09˚, N–Cu2–Br 106.54˚, S–Cu2–Br 120.99˚.

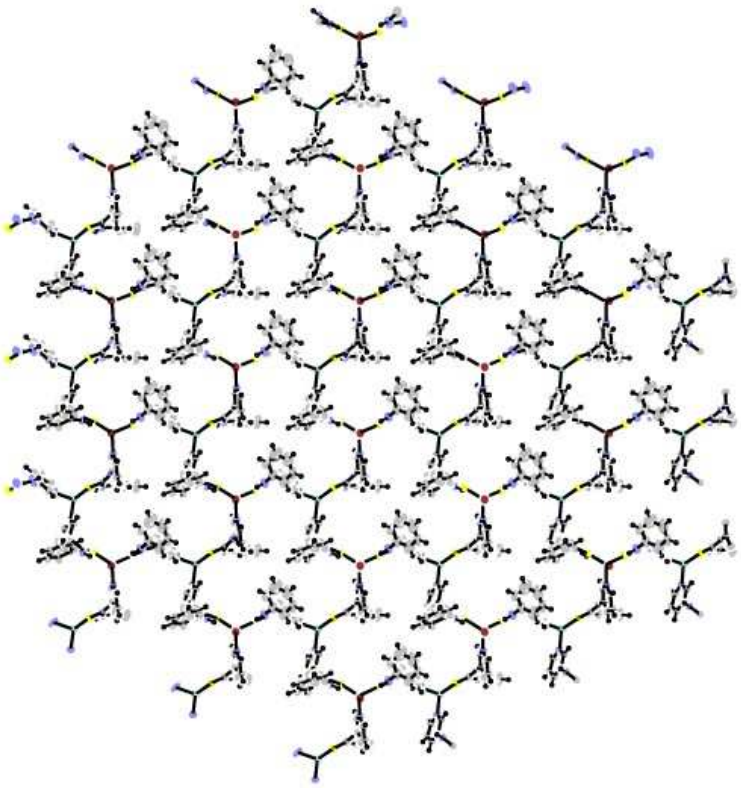

Figure 27: $(CuBr)_2(3\text{-}PyTuPh)_3$ sheet structure

As indicated in Figure 26, both copper atoms achieve their preferred coordination number of four. The phenyl group is not involved in the bonding of copper(I) resulting in nearly perpendicular orientation to the 2-dimensional sheet structure shown in Figure 27. Similarly, the bromide coordinates a single copper, and so is oriented perpendicular to the plane of the sheet. The sheet geometry results in the appearance of small holes, surrounded by six thioureas. The presence of such vacancies suggest that this structure could have potential applications as a small molecule carrier.

3.2.2.6 $CuBr(BztTuMe)_2$

Crystals of $CuBr(BztTuMe)_2$ were grown from 20 mM CuBr in acetonitrile layered with 20 mM (BztTuMe) in acetone. The structure obtained is shown in Figure 28.

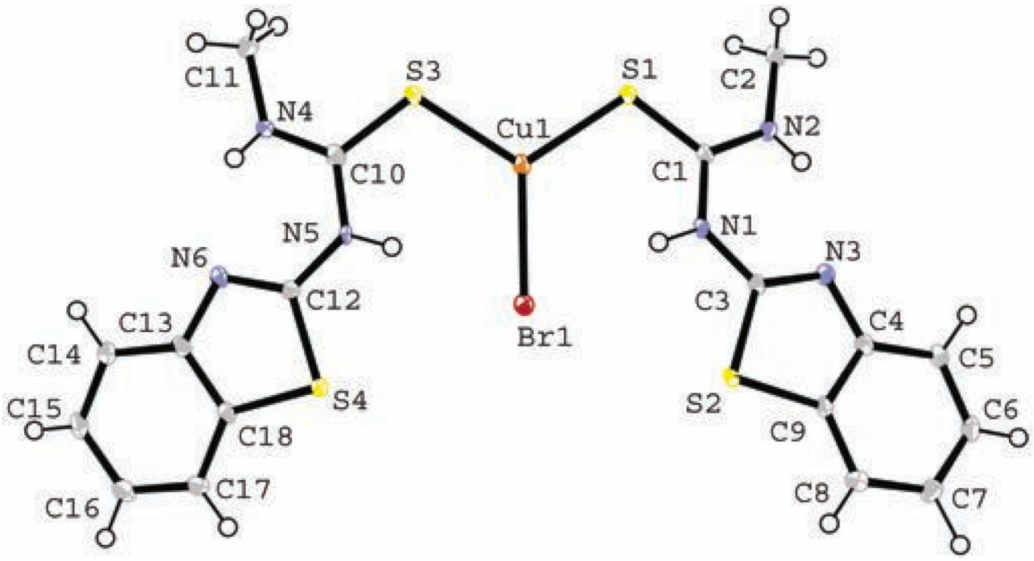

Figure 28: $CuBr(BztTuMe)_2$ molecular diagram

Like the $CuCl(PymTuPh)_2$, and the $CuCl(PymTuMe)_2$ complexes, the $CuBr(BztTuMe)_2$ complex consists of a three-coordinate central copper atom bonded to a bromine atom and two sulfur atoms. Each sulfur atom is provided by a single BztTuMe thiourea. Though the complex shows trigonal planar geometry around the copper atom, the bond angles are significantly distorted from the ideal value of 120˚. The bond angles were found to be: S–Cu–S 114.72˚, S–Cu–Br 122.41˚. One hypothesis for the S–Cu–S bond angle being squeezed well below the expected 120˚ involves the presence of lone pairs of electrons around the two sulfur atoms on the 2-aminobenzothiazole rings. Lone pairs of electrons occupy more space, thus pushing the Cu-S bonds away from them, thus leading to a shorter S–Cu–S bond angle. Selected bond lengths around the copper atom were found to be: Cu–Br 2.4216 Å, Cu–S 2.2355 Å. The structure did not show any intermolecular interactions.

3.2.2.7 $(CuI)_2(PymTuMe)_2$

$(CuI)_2(PymTuMe)_2$ crystals were prepared by layering 20 mM PymTuMe in CH_2Cl_2 onto 20 mM CuI in MeCN. The resulting structure is shown in Figure 29 and 30.

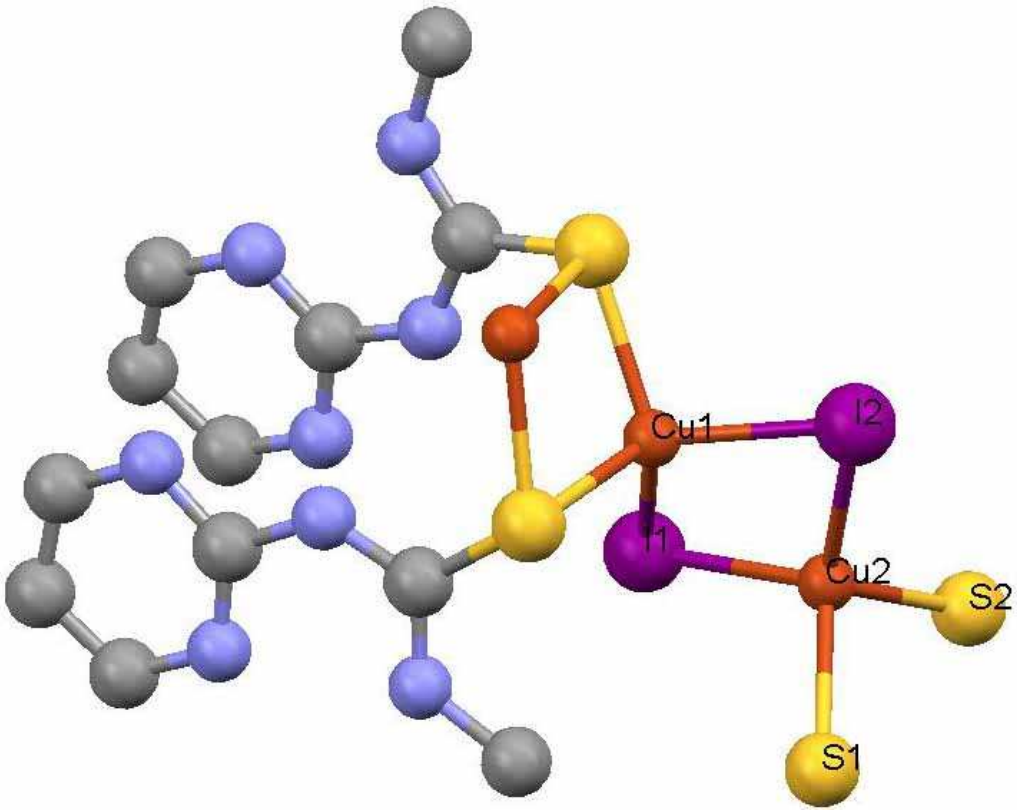

Figure 29: $(CuI)_2(PymTuMe)_2$ molecular diagram. Hydrogen atoms omitted for clarity.

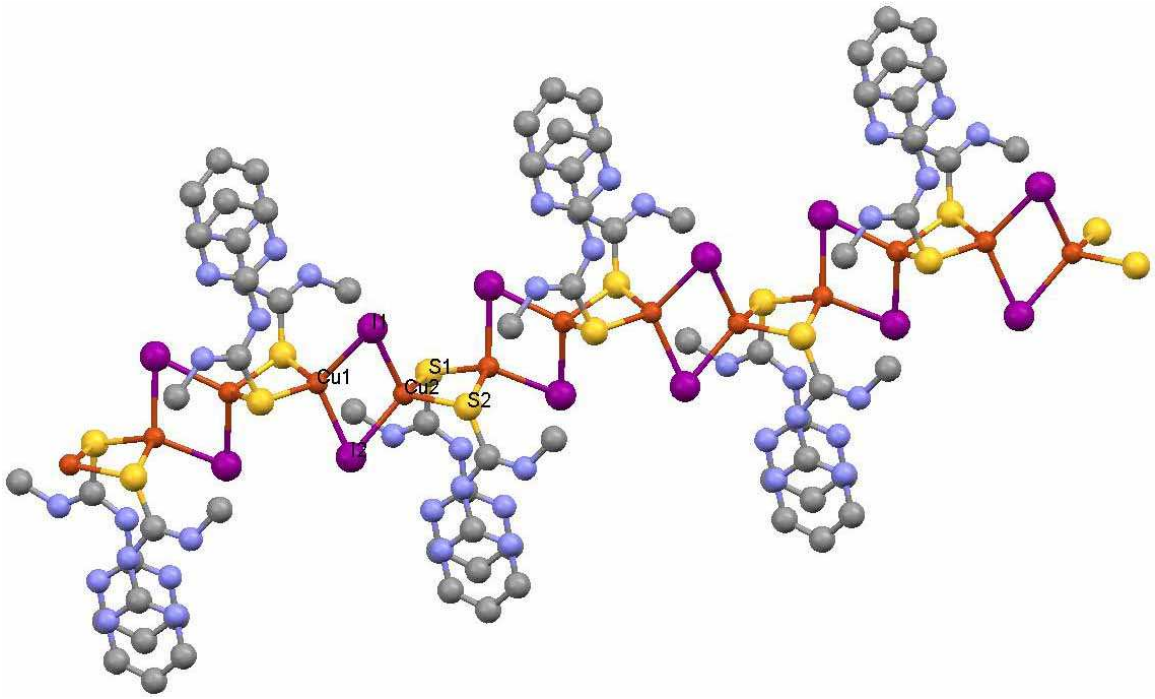

Figure 30: $(CuI)_2(PymTuMe)_2$ chain structure. Hydrogen atoms omitted for clarity.

Here, copper(I) is four-coordinate with a pseudotetrahedral geometry. Each copper atom coordinates to two sulfurs, two iodides. Interestingly, each ligand is bridging, coordinating two copper atoms into rhomboid dimers that show a weak Cu–Cu interaction (2.935Å). Shared μ_2-I centers create a second series of dimer units which feature a slightly stronger Cu–Cu interaction (2.793 Å). These pairs of dimers share copper atoms to produce a chain. The chain is not linear, but rather ripples as it propagates in one dimension. Selected bond angles around the copper atoms were found to be: Cu1–I1–Cu2 64.057°, S1–Cu1–S2 102.79°, I1–Cu1–I2 113.65°. One might expect the bulky pyrimidyl rings to orient themselves on opposite sides of the sulfurs so as to maximize the distance between them, but in actuality, they lie adjacent to each other. This behavior is an example of so-called π-stacking, in which the π-electrons associated with the aromatic rings interact. The short (3.552 Å) distance between the ring centroids

is indicative of π-stacking. The interaction of these adjacent rings appears to cause the rippling of the ...Cu(η_2-I)$_2$Cu(η_2-S)$_2$... chains.

3.2.2.8 CuI(BztTuMe)

Crystals for CuI(BztTuMe) were grown by layering 20 mM BztTuMe in MeCN onto 20 mM CuI in MeCN. The crystal structures are shown below in Figures 31 and 32. Each copper is equivalent and is bound to two sulfurs, two iodines, and also contains a Cu–Cu interaction.

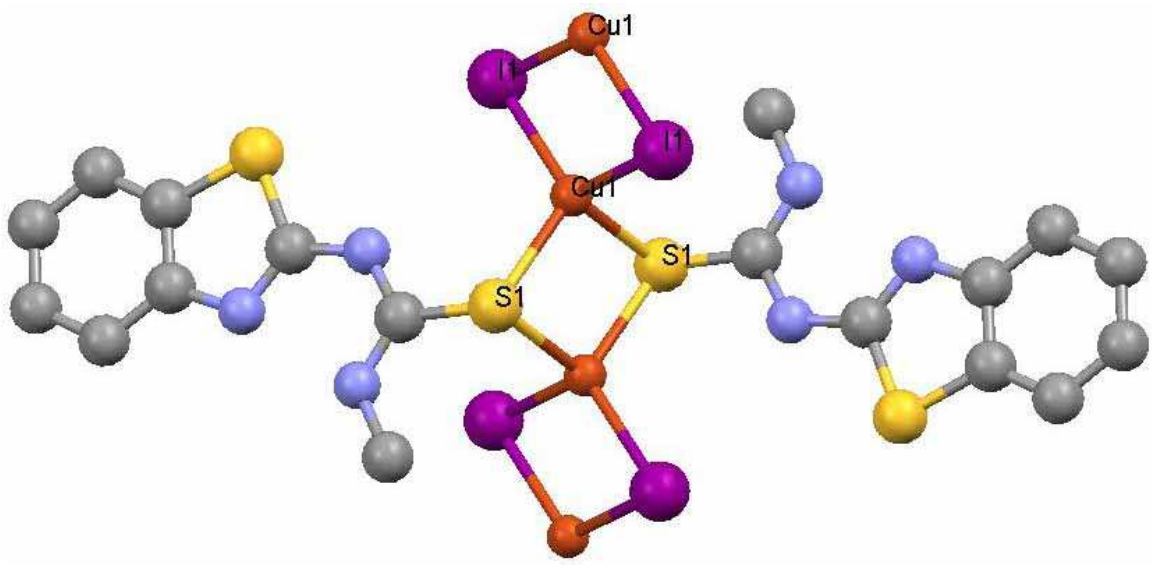

Figure 31: CuI(BztTuMe) molecular diagram. Hydrogen atoms omitted for clarity.

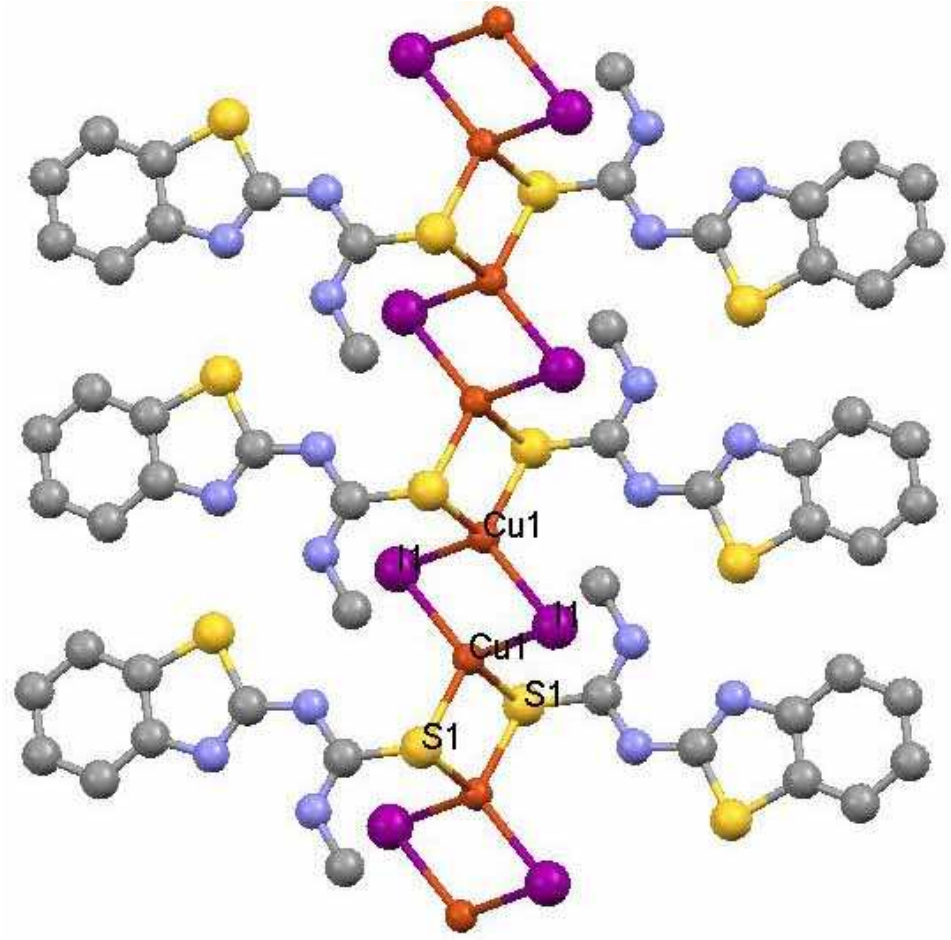

Figure 32: CuI(BztTuMe) chain structure. Hydrogen atoms omitted for clarity.

Selected bond lengths were found to be: bonded Cu–Cu 2.7194 Å, non-bonded Cu–Cu 3.0171 Å, Cu–I 2.6553 Å, Cu–S 2.3185 Å. Thus, there is apparent interaction between the non-bonded copper atoms. The CuI(BztTuMe) polymer forms a one-dimensional chain consisting of two alternating rhombic units. One of them consists of two copper atoms bonded to two iodine atoms and to each other. The second unit consists of two copper atoms coordinating with two sulfur atoms located on two separate thioureas which cap the linear chain. Selected bond angles were found to be: S–Cu–S 101.06°, I–Cu–I 117.87°.

3.2.2.9 [Cu(3-PyTuPh)$_2$]NO$_3$

The crystal for $[Cu(3\text{-}PyTuPh)_2]NO_3$ was prepared by layering 20 mM 3-PyTuPh in MeCN onto a MeCN solution containing roughly 20 mM $CuNO_3$. The concentration of copper(I) nitrate was approximate because the copper was reduced from copper(II) nitrate. However, a solvable crystal was produced, and the resulting structure is shown in Figures 33 and 34.

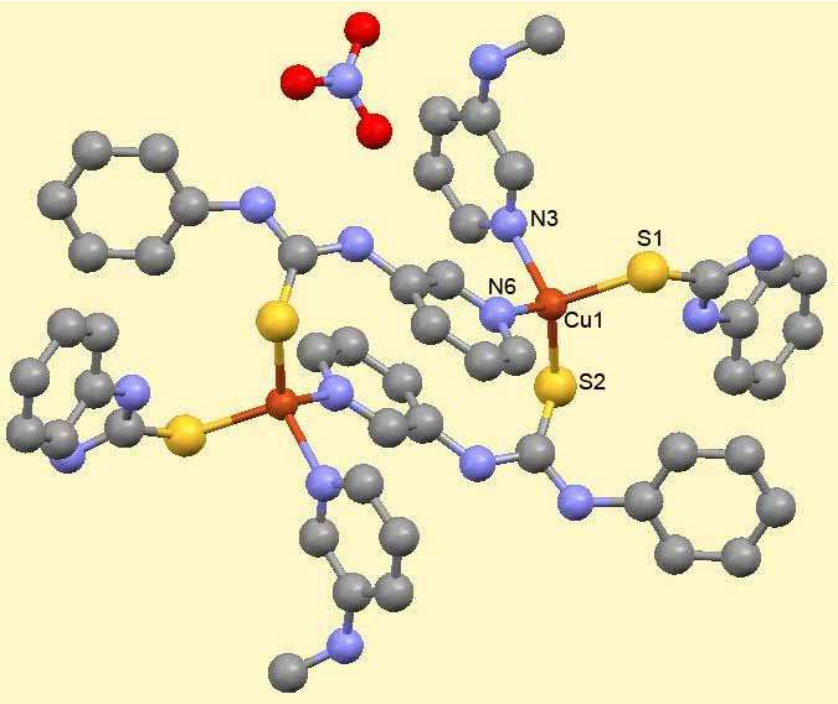

Figure 33: $[Cu(3\text{-}PyTuPh)_2]NO_3$ molecular diagram. Hydrogen atoms omitted for clarity.

Selected bond lengths were found to be: Cu–S 2.2792 Å, and Cu–N 2.0629 Å. Selected bond angles around copper were found to be: N6–Cu1–S1 101.16°, N6–Cu1–N3 101.02°, N6–Cu1–S2 118.90°, N3–Cu1–S2 111.48°, N3–Cu1–S1 106.99°, S2–Cu1–S1 115.614°.

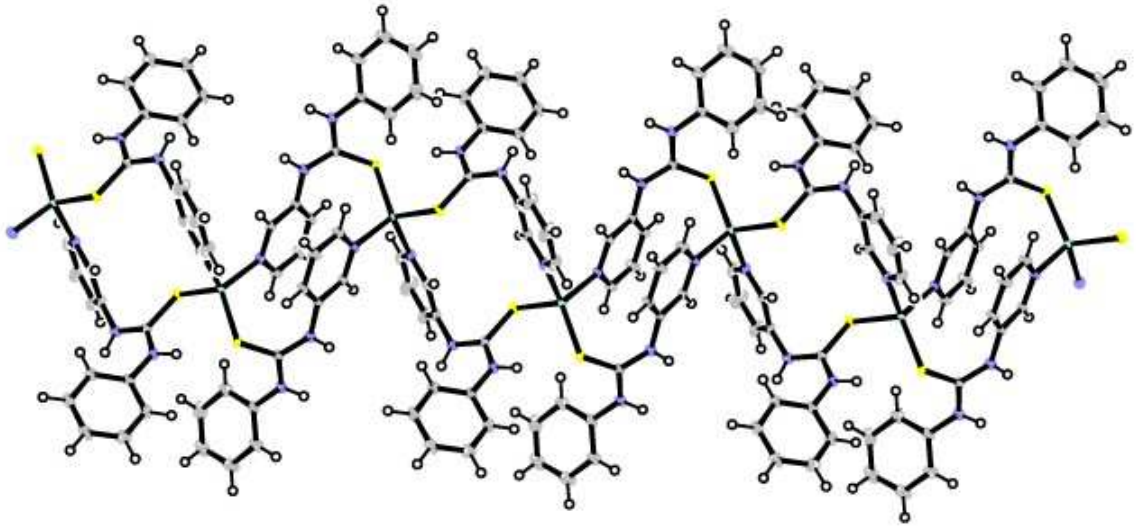

Figure 34: $[Cu(3\text{-}PyTuPh)_2]NO_3$ chain structure

The structure in Figure 34 is the first here considered where the anion (nitrate) is not coordinated directly to the copper atom. This non-coordinating behavior is much more common for nitrate than it is for halide. Copper(I) is able to assume its four-coordinate geometry by coordinating two sulfurs and two pyridyl nitrogen atoms. Like CuI(PymTuMe), $[Cu(3\text{-}PyTuPh)_2]NO_3$ forms a long chain of interlocking ring units that share copper centers. Each dimer unit is formed by two thioureas bridging two copper atoms. The binding of the nitrogen atoms forces the phenyl and pyridyl rings on each thiourea to assume orientations roughly perpendicular to each other. The pyridyl rings within the macrocyclic dimer (Figure 34) ring show clear evidence of π-stacking, as the centroid–centroid distance is just greater than is found for $(CuI)_2(PymTuMe)_2$, namely, 3.618 Å.

3.2.2.10 $[Cu\{(2\text{-}Py)_2Tu\}_2]NO_3$, $(CuNO_3)_2(patp)_2$•MeCN

The crystals for $[Cu\{(2\text{-}Py)_2Tu\}_2]NO_3$ and $(CuNO_3)_2(patp)_2$•MeCN were prepared by layering 20 mM $(2\text{-}Py)_2Tu$ in MeCN onto a MeCN solution containing roughly 20 mM

$CuNO_3$. The concentration of copper(I) nitrate was approximate because the copper was reduced from copper(II) nitrate. However the crystal tube showed growth of yellow and orange colored crystals. Both crystals produced solvable structures and are discussed below. The structure resulting from solving the orange crystals are shown in Figures 35 and 36.

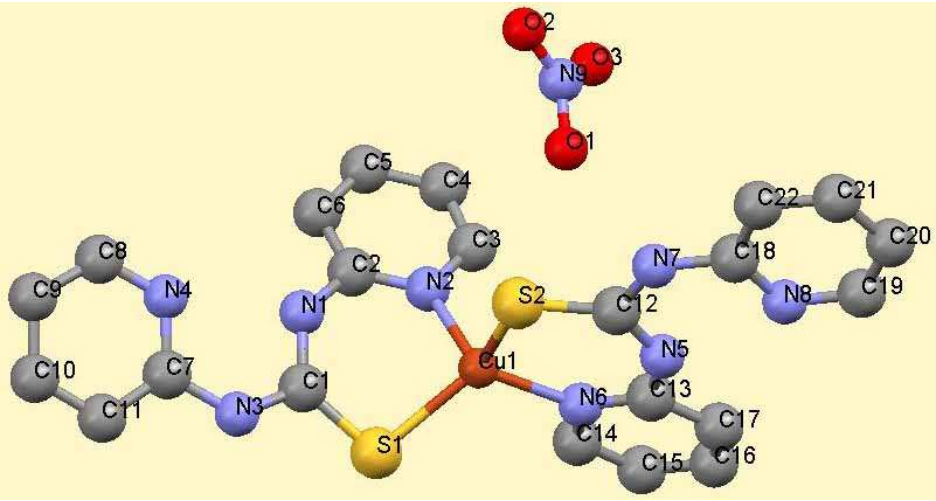

Figure 35: $[Cu\{(2\text{-}Py)_2Tu\}_2]NO_3$ molecular diagram. Hydrogen atoms omitted for clarity. Selected bond lengths around the copper atom were found to be: Cu1–S1 2.2846 Å, Cu1–S2 2.2178 Å, Cu1–N2 2.0954 Å, Cu1–N6 2.0069 Å. Selected bond angles around copper atom were found to be: N6–Cu1–N2 109.15°, N6–Cu1–S2 101.16°, N6–Cu1–S1 115.55°, N2–Cu1–S2 108.53°, N2–Cu1–S1 91.67°, S2–Cu1–S1 129.35°. Thus, this complex has a roughly tetrahedral geometry with the copper atom coordinating four atoms: a sulfur and nitrogen atom from one thiourea, and another sulfur and nitrogen atom from another thiourea. The nitrate ion hydrogen-bonds to a thiourea nitrogen atom, forming a one-dimensional chain structure, see Figure 36.

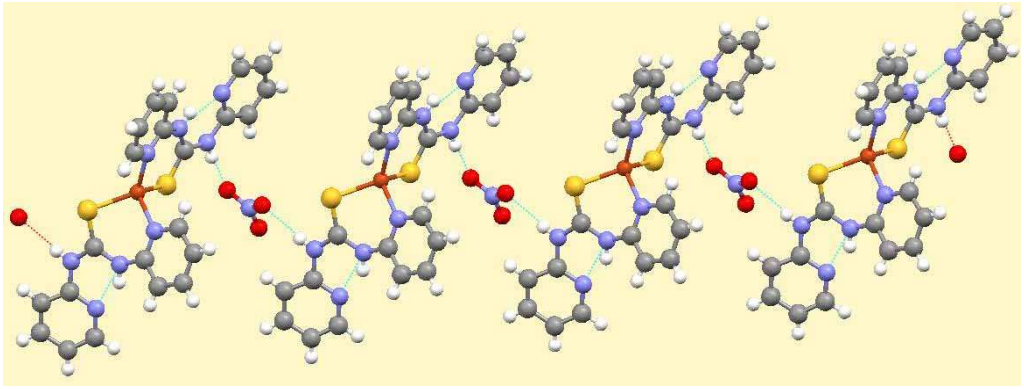

Figure 36: $[Cu\{(2\text{-}Py)_2Tu\}_2]NO_3$ showing H-bonding interactions

The two thioureas cap the chain on either side. Inter- and intramolecular H-bonding is seen. The hydrogen atom on one of the thiourea nitrogen atoms participates in H-bonding with the nitrate molecule. Also, intramolecular H-bonding is seen between two nitrogen atoms in both thioureas.

The structure resulting from solving the orange crystals are shown in Figures 37.

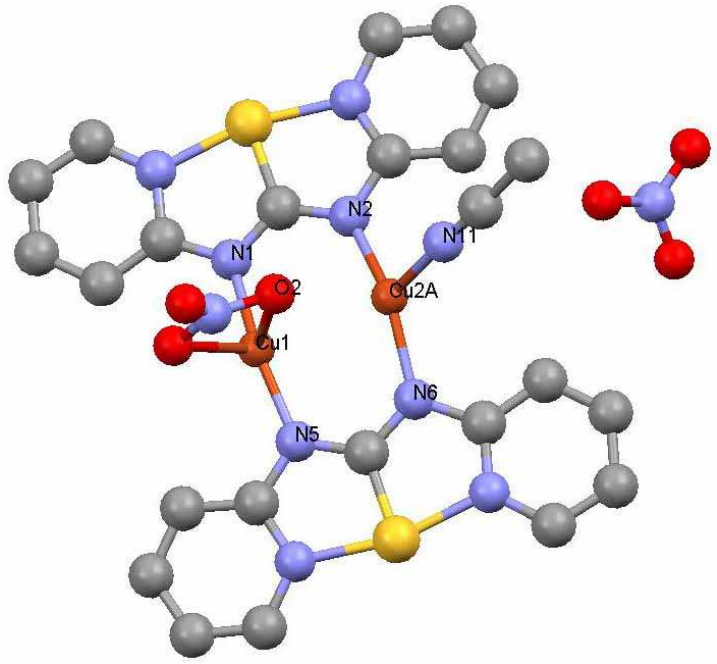

Figure 37: $(CuNO_3)_2(patp)_2$•MeCN molecular diagram. Hydrogen atoms omitted for clarity.

As can be seen in Figure 37, the $(2\text{-Py})_2\text{Tu}$ ligand cyclizes to form dipyridyltetraazathiapetalene which coordinates with copper atoms through the lone pair of electrons on the thiourea nitrogen atoms. Cu1 and Cu2 are three coordinate. Cu1 coordinates to an oxygen atom on a nitrate anion, and to two nitrogen atoms: one on each of the two ligands. Cu2 coordinates to a nitrogen atom from MeCN, and to two nitrogen atoms: one on each of the two ligands Selected bond lengths around the copper atoms were found to be: Cu2-N6 1.971 Å, Cu2-N11 2.103 Å, Cu1-N1 1.916 Å, Cu1-O2 2.588 Å. Selected bond angles around copper atoms were found to be: N2-Cu2-N6 152.29°, N11-Cu2-N6 106.01°, Cu2-Cu1-O2 69.54°, N5-Cu1-Cu2: 87.14°. This cyclized complex does not show any hydrogen-bonding. Its packing structure is seen in Figure 38.

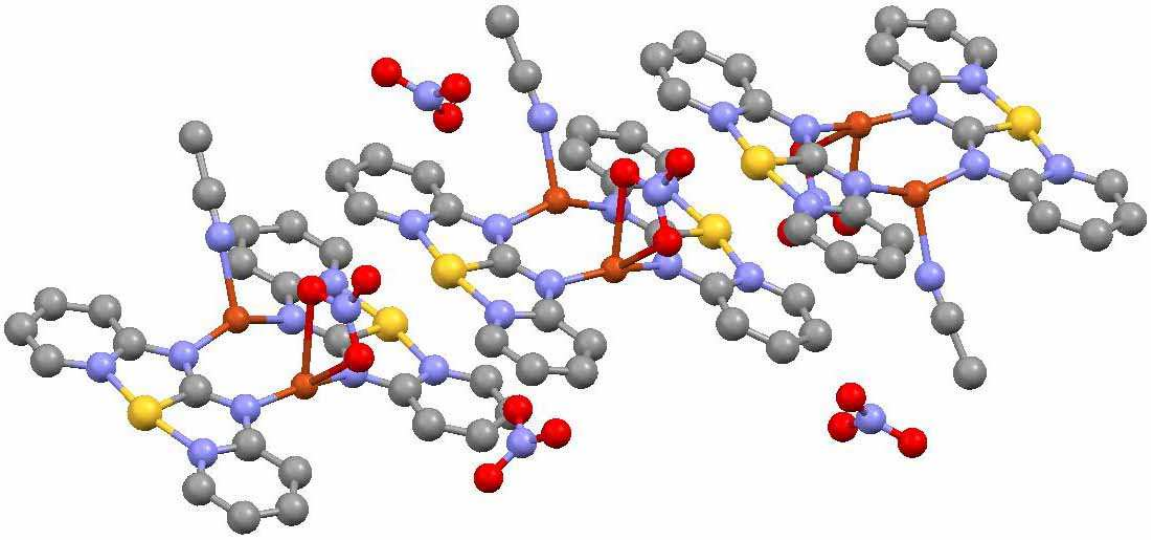

Figure 38: $(CuNO_3)_2(patp)_2$•MeCN packing diagram. Hydrogen atoms omitted for clarity.

Interesting to note from this structure is the way the complex packs so as to remove spaces and voids. Also, a clear case of π-stacking can be seen. The distance between the two rings was found to be 3.574 Å.

4. Conclusion

Several novel heterocyclic thioureas were synthesized. When crystalline material could be obtained, X-ray crystallography was used to describe the structure and intermolecular forces relevant to each thiourea. The use of 3- or 4-pyridyl groups in thioureas serves to produce 1D, 2D or 3D networked products through intermolecular hydrogen-bonding. 2-Pyridyl, 2-pyrimidyl, and 2-thiazolyl groups lead to the formation of dimers containing both intra- and intermolecular hydrogen-bonds.

Several novel copper(I) thiourea complexes of the form $(CuX)_x(RNHCSNHR')_y$ (X = Cl, Br, I, or NO_3; R = 2-pyridyl, 3-pyridyl, pyrimidyl, thiazole or benzothiazole; and R′ = 2-pyridyl, 3-pyridyl, phenyl, or methyl) were synthesized. It is hoped that these complexes may be able to coordinate small molecules useful in biological systems or act as catalysts. Atomic absorption spectroscopy revealed a variety of molar ratios, even when reactions were carried out under equimolar conditions. X-ray crystallography, when crystalline material could be obtained, was used to describe the structure and intermolecular forces relevant to each complex. $CuCl(PymTuPh)_2$, $CuCl(PymTuMe)_2$, and $CuBr(BztTuMe)_2$ gave monomeric structures where two thioureas were bound by copper. $CuBr(2\text{-}PyTuPh)_2$, $(CuI)_2(PymTuMe)_2$, CuI(BztTuMe), $[Cu(3\text{-}PyTuPh)_2]NO_3$, and $[Cu\{(2\text{-}Py)_2Tu\}_2]NO_3$ gave one-dimensional linear chains. $(CuCl)_2[(2\text{-}Py)_2Tu]_2$ and $(CuBr)_2(3\text{-}PyTuPh)_3$ gave two-dimensional sheet-like structures. The incorporation of additional nitrogen and sulfur atoms on ligand molecules, for example, pyrimidyl, thiazole, and benzothiazolyl rings; was hoped would produce additional coordination sites for copper thus leading to more complex structures. Most surprising was the knowledge that none of the eleven copper(I) complexes produced a three-dimensional

structure. Infact, as noted above, $CuCl(PymTuPh)_2$, $CuCl(PymTuMe)_2$, and $CuBr(BztTuMe)_2$ gave monomeric structures. $(CuCl)_2[(2\text{-}Py)_2Tu]_2$, $(CuI)_2(PymTuMe)_2$, CuI(BztTuMe), and $[Cu\{(2\text{-}Py)_2Tu\}_2]NO_3$ did not produce three-dimensional structures as was hoped.

The reaction of $CuNO_3$ with $(2Py)_2Tu$ gave interesting results. Based on our hypothesis, an isolatable intermediate, $(CuNO3)_2[(2\text{-}Py)_2Tu]_3$•MeCN, is formed which then forms the $[Cu\{(2\text{-}Py)_2Tu\}_2]NO_3$ kinetic product. Upon further standing, as was in the case of crystal growth, this structure cyclizes to form the thermodynamically favorable $(CuNO_3)_2(patp)_2$•MeCN. Further studies needs to be done to confirm this hypothesis.

5. References

1. Tobe, Y.; Sasaki S.-I.; Mizuno M.; Hirose, K.; Naemura, K. *J. Org. Chem.* **1998**, *63*, 7481. (b) Succaw, G. L.; Weakley T. J. R.; Han, F.; Doxsee, K. M. *Cryst. Growth Des.* **2005**, *5*, 2288.
2. Yutronic, M.; Manriquez, V.; Jara, P.; Witke, O.; Merchán, J.; Gonzáles, G. *J. Chem. Soc., Perkin Trans. 2* **2000**, 1757. (b) Babb, J. E. V.; Burke, N. J.; Burrows, A. D.; Mahon, M. F.; Slade, D. M. K. *Cryst. Eng. Comm.* **2003**, *5*, 226.
3. Rudd, M. D.; Lindeman, S. V.; Husebye, S. *Phosphorus Sulfur Silicon Relat. Elem.* **1997**, *123*, 313.
4. Angelova, O.; Kossev, K.; Atanasov, V. *Acta Crystallogr. Sect. C* **1999**, *55*, 220.
5. West D. X.; Hermetet, A. K.; Ackerman, L. J.; Valdes-Martinez, J.; Hernandez-Ortega, S. *Acta Crystallogr. Sect. C* **1999**, *55*, 811. (b) Valdes-Martinez, J.; Hernandez-Ortega, S.; West, D. X.; Ackerman, L. J.; Swearingen, J. K.; Hermetet, A. K. *J. Mol. Struct.* **1999**, *478*, 219. (c) Kaminsky, W.; Goldberg, K. I.; West, D. X. *J. Mol. Struct.* **2002**, *605*, 9.
6. Venkatachalam, T; Sudbeck, E; Uckun, F. *J. Mol. Struct.* **2004**, 45, 687.
7. Tellez, F; Cruz, A; Lopez-Sandoval, H; Ramos-Garcia, I; Gayosso, M; Castillo-Sierra, R; Paz-Michel, B; Noth, N; Flores-Parra, A; Contreras, R. *Eur. J. Org. Chem.* **2004**, 4203.
8. Tsogoeva, S; Hateley, M; Yalalov, D; Meindl, K; Weckbecker, C; Huthmacher, K. *Bioorg. Med. Chem.* **2005**, 13, 5680.

9. Zhong, H-P; Long, L-S; Huang, R-B; Zheng, L-S; Ng, S. *Acta. Crystallogr. Sect. C*. **2003**, 59, 1596.
10. Allen, F; Bird, C; Rowland, R; Raithby, P. *Acta. Crystallogr. Sect. B*. **1997**, 53, 680.
11. Cotton, A. *Advanced Inorganic Chemistry.* Fifth ed. New York: Wiley, 1988.
12. Robson, R; Batten, S. *Angew. Chem. Int.*, **1998**, 37, 1460.
13. Beatty, Alicia M. *Coordination Chemistry Reviews*, **2003**, 246, 131.
14. Pike, R; Wiles, A. *Organometallics*. **2006**, 25, 3282.
15. Pike, R; Graham, P; Sabat, M; Bailey, R; Pennington, W. *Inorg. Chem.* **2000**, 39, 5121.
16. Pike, R; Kuperstock, J. *Unpublished data*.
17. Janiak, C. *J. Chem. Soc., Dalton Trans.* **2000**, 3885.
18. SAINT+, Bruker Analytical X-ray Systems. Madison, WI. **2001.**
19. SADABS, Bruker Analytical X-ray Systems. Madison, WI. **2001.**
20. Sheldrick GM SHELXTL, Crystallographic Computing System, Version 6.12, Bruker Analytical X-ray Systems. Madison, WI. **2001.**
21. Mercury 1.4.2, Cambridge Crystallographic Data Centre. Cambridge, UK. **2007**.
22. Hansen, E; Petersen, H. *Synth. Commun.* **1984**, 14, 537.
23. Manley, P; Quast, U. *J. Med. Chem.* **1992**, 35, 2327.
24. Deady, L; Ganame, D; Hughes, A; Quazi, N; Zanatta, S. *Aust. J. Chem.* **2002**, 55, 287.
25. Fan, Y; Lu, H; Hou, H; Zhou, Z; Zhao, Q; Zhang, L; Cheng, F. *J. Coord. Chem.* **2000**, 50, 65.

26. Yamaguchi, K; Shudo, K. *J. Agric. Food. Chem.* **1991**, 39, 793.

27. Corbin, P; Zimmerman, S. *J. Am. Chem. Soc.* **2000**, 122, 3779.

28. Kumar, D; Jose, D; Das, A; Dastidar, P. *Chem. Commun.* **2005**, 4059.

29. Huang, R. *Journal of Molecular Structure*. **2002**, 610, 265.